

Department of Precision and Microsystems Engineering

Thin-walled Warping Beams for Differential Mechanism Applications

Maurice Corné Valentijn

Report no : 2020.044  
Coach : Dr. ir. G. Radaelli & ir. A. Amoozandeh Nobaveh  
Professor : Prof. dr. ir. J.L. Herder  
Specialisation : MSD  
Type of report : Thesis  
Date : 26 October 2020





# Thin-walled Warping Beams for Differential Mechanism Applications

by

Maurice Corné Valentijn

to obtain the degree of Master of Science  
at the Delft University of Technology,  
to be defended publicly on Monday October 26, 2020 at 14:00.

Student number: 4387511  
Project duration: September 24, 2019 – October 26, 2020  
Thesis committee: Prof. dr. ir. J.L. Herder, TU Delft, supervisor, chair  
Dr. ir. J.F.L. Goosen, TU Delft  
Dr. ir. G. Radaelli, TU Delft, daily supervisor  
ir. A. Amoozandeh Nobaveh, TU Delft, daily supervisor

*This thesis is confidential and cannot be made public until October 01, 2021.*

An electronic version of this thesis is available at <http://repository.tudelft.nl/>.



# Preface

Now that I have come to the beginning of the end, writing the "pre"-face at the finish of the hard work feels kind of ironic. This preface does not only mark the end of my thesis or my master PME, but the end of 6 and a bit years of studying at the university. I would have never imagined that the end of my student life is coming to an end, but I am grateful for every minute. I learned a lot of new skills, collected a lot of knowledge but most importantly, I got to know a lot of bright and amazing people without whom I would have never gotten this far.

I would like to start with thanking my supervisors Giuseppe and Ali for all the fruitful discussions and great enthusiasm you both possess, you guys can be proud of the environment you created within the group. Then to the shellskeleton research group itself, thank you for all the discussions and keep up the good work!

A huge thanks to the technical support team of PME, always there to help and have a laugh. Thanks to my friends and the critical reviewers for the coffee moments and feedback along the way. And last but not least my family and girlfriend whom without, this would not have been possible.

So without any further ado, and with great enthusiasm, I hereby present my thesis project. I hope you enjoy it as much as I did during most of the time.

*Maurice Valentijn  
Delft, October 2020*



# Abstract

The objective of this thesis is to show that warping can be used in a thin-walled beam to create a suitable replacement for a classical differential mechanism. This normally negated deformation of the cross section can be used to create an inverse transmission mechanism, used to create a monolithic and simple alternative to a classic differential mechanism. This warping beam differential mechanism can be used to add walking functionality to a back support passive exoskeleton. These exoskeletons are optimized to reduce muscle stress during lifting, but this comes with the downside of an increase in muscle activity during walking. To counter this increase in muscle activity, the use of a differential mechanism is suggested.

To show the feasibility of the proposed solution, a characterization of the warping beam differential mechanism is made for different geometric properties. This characterization is done with respect to two functionalities, to determine the geometric advantage of the inverse transmission and the rotational compliance under torque of the beam. The warping constant and torsion constant are determined to be the geometric properties of most influence on the behaviour of the warping beam. It is also shown that within the proposed boundary conditions, different beam cross sections with the same geometric properties show the same behaviour. An increase in warping constant results in an increase in geometric advantage and a reduction of the rotational compliance. The torsion constant has a linear correlation to the stored energy for the inverse transmission functionality, having less influence on the geometric advantage and rotational compliance compared to the warping constant.

This thesis shows that this new kind of differential mechanism can be used to replace the classical mechanism and the potential can be seen with an achieved theoretical geometric advantage of almost 1. A systematic overestimation of the geometric advantage and an underestimation of the compliance is made by the model with respect to the experiments, but with some improvements this theoretical goal is not far away.



# Contents

<b>1</b>	<b>Introduction</b>	<b>1</b>
1.1	Thesis objective . . . . .	3
1.2	Thesis outline . . . . .	3
<b>2</b>	<b>Paper : Warping in thin-walled structures for differential mechanism applications</b>	<b>5</b>
<b>3</b>	<b>Additional results</b>	<b>17</b>
3.1	Experiment data . . . . .	17
3.2	Stress analysis . . . . .	20
<b>4</b>	<b>Discussion</b>	<b>21</b>
4.1	Experimental data . . . . .	21
4.2	Stress analysis . . . . .	22
4.3	Future work . . . . .	22
<b>5</b>	<b>Conclusion</b>	<b>23</b>
	<b>Bibliography</b>	<b>25</b>
<b>A</b>	<b>Literature study</b>	<b>27</b>
<b>B</b>	<b>Warping theory</b>	<b>49</b>
B.1	Warping displacement . . . . .	50
B.2	Torsion formula . . . . .	51
B.3	Torsion stresses . . . . .	51
B.4	Warping stiffness . . . . .	52
B.5	Twist. . . . .	52
<b>C</b>	<b>Test setup</b>	<b>55</b>
C.1	Load case 1. . . . .	55
C.2	Load case 2. . . . .	55
<b>D</b>	<b>Matlab and Ansys code</b>	<b>59</b>



## Introduction

To reduce the work load or to increase endurance of a work force, industries are increasingly utilizing exoskeletons to aid employees. These exoskeletons can be categorized into active or passive exoskeletons [17]. No external energy source is used to power passive exoskeletons, making them self-sufficient, thereby differing from their active counterpart.

Different applications exist for passive exoskeletons, such as arm, leg or back support. Back support exoskeletons work by storing energy while bending over, then utilizing this energy to aid the wearer while standing up. Companies like Laevo and SuitX create such exoskeletons, both adopting this design philosophy.

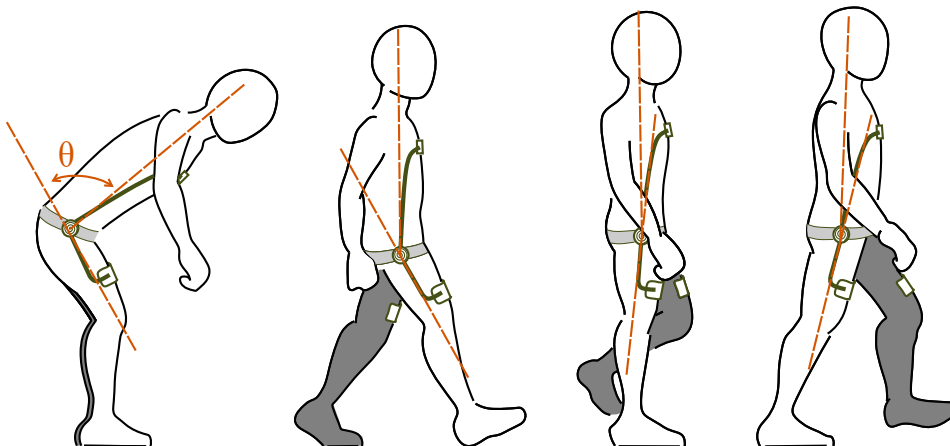


Figure 1.1: An illustrations of both a lifting position and walking poses, with the passive exoskeleton shown.  $\theta$  depicts the relative angle between the upper torso and upper legs.

Figure 1.1 shows such an exoskeleton and the position on a body. From each hip, a support goes to the chest and another goes to the upper leg. The first pose shows the bent position, in which energy is stored in both hip joints relative to angle  $\theta$ . This stored energy is used to assist the wearer during lifting, lowering the load on the back muscles. Studies into the Laevo exoskeleton show a decrease in back muscle activity during lifting [1, 4].

However, an increase in muscle activity during walking is measured, accompanied by a larger amount of discomfort [1, 4]. This problem is illustrated by the walking positions shown in Figure 1.1. It can be seen that the angle  $\theta$  does not stay zero during walking, indicating a storage of energy during gait. It should also be noted that the stored energy during walking is different for each leg, adding discomfort.

To counter this increase in muscle activity, a coupling between the legs is proposed to cancel this energy built-up during walking while still aiding the upper body during lifting. A differential mechanism

is proposed to create this kinematic behaviour as it fits the natural behaviour of the legs during walking while coupling the two legs to store energy during lifting. A differential mechanism is defined by IFToMM as "Mechanism for which the degree of freedom is two and which may accept two inputs to produce one output or may resolve a single input into two outputs" [8].

For a conventional differential mechanism, these two Degrees of Freedom (DoF) can be dedicated to the two different functionalities. An example of a differential mechanism used in a car can be seen in Figures 1.2 and 1.3. Both figures depict the internal DoFs resulting in a single external DoF. Red colored arrows are constraint, green are applied rotations and yellow are resultant rotations. Figure 1.2 shows the outer gear being locked, creating an inverse transmission shown as DoF 1. Figure 1.3 depicts DoF 2, with a single moment input on the outer gear resulting in an equally distributed output moment on both shafts.

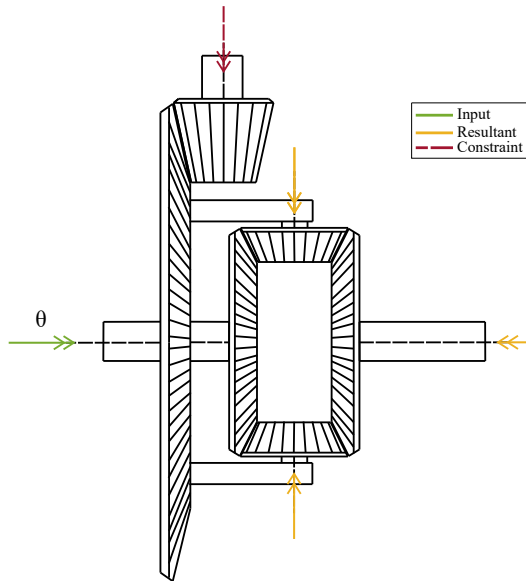


Figure 1.2: Functionalities of a classic differential mechanism with Degree of Freedom 1 being depicted.

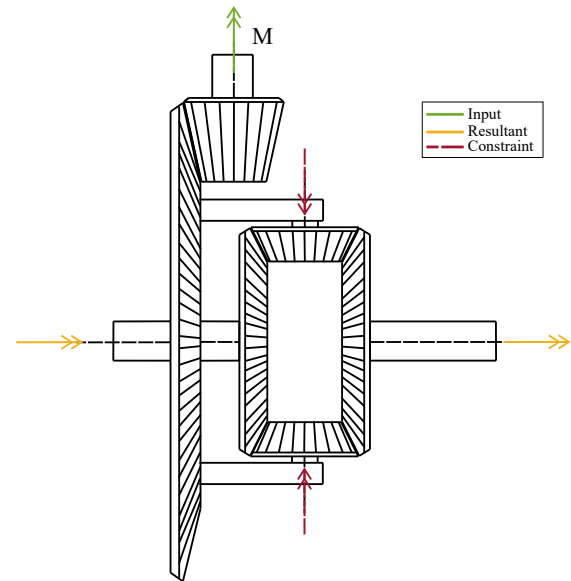


Figure 1.3: Functionalities of a classic differential mechanism with Degree of Freedom 2 being depicted.

A characterization of differential and remote center of rotation mechanisms is done to find possible solutions or gaps in literature to apply to a passive lifting exoskeleton, seen in Appendix A. All two DoF mechanisms are considered in characterizing a differential mechanism, as the IFToMM definitions has no restrictions. Remote center of rotation mechanisms are also characterized, with the goal to aid comfort by alignment of the exoskeleton with respect to the human movement.

These conventional differential mechanisms do have shortcomings like play, assembly, wear and possibly weight. To solve these shortcomings, a compliant shell mechanism is proposed to function as a differential mechanism. In accordance with Nijssen, "Compliant shell mechanisms are spatially curved thin-walled structures able to transfer or transit, force, motion or energy through elastic deformation" [12].

To gain differential mechanism functionality for a compliant mechanism, warping is utilized. Warping, or warping displacement, is the out-of-plane deformation of the cross section and occurs when torque is applied to a thin-walled beam [18]. This applied torque causes shear stress and consequent shearing strain to develop in the cross sec-

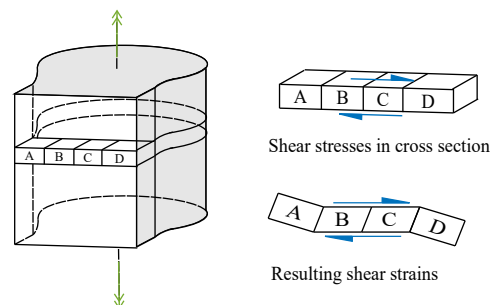


Figure 1.4: Visualization of warping in non-cylindrical beam. The applied torque create shear stresses in the cross section, causing shear strain. adapted from Oden and Ripperger (1981) [13].

tion (CS). If Figure 1.4 is considered, elements  $B$  and  $C$  develop these stresses and thereby deform. This does not hold for elements  $A$  and  $D$ , resulting in a rotation of the element and a subsequent out of plane displacement of the CS called warping [13]. Further explanation on warping can be found in Appendix B.

Studies have been done into the transmission of warping through beams and through beam joints and connections [2, 3, 15], with the goal to predict and nullify this warping behaviour. The contrary is of interest now as, next to exoskeletons, it could also serve as a solution for different engineering fields benefiting from monolithic parts.

## 1.1. Thesis objective

To take the first step towards implementation into industry, the practicality of using warping needs to be investigated. To give insight into this feasibility, the research goal is defined as:

*"Characterizing the behaviour of a warping beam as differential mechanism for different geometric properties".*

## 1.2. Thesis outline

The thesis starts out with a paper in Chapter 2, presenting the characterization of the warping beam differential mechanism. The paper includes an overview of the theory on warping from which the important geometric properties are selected. The method section shows the experimental setup, used beams during the tests, considered boundary conditions, material choices and used ANSYS models. The results of the paper show the comparison of analytical and finite element models with the experimental results and the contour plots made to characterize the beam functionalities over a range of geometric property values. Chapter 3 shows the raw experimental data over a range of input rotation angles and input torque and a general stress analysis. Chapter 4 and 5 discuss the additional results and conclude on the total thesis. Supplementary material is given in the appendices, showing the literature study, warping theory, test setup and MATLAB and ANSYS APDL code.



# 2

## Paper : Warping in thin-walled structures for differential mechanism applications

This chapter presents the research in a paper format. The essentials on the theory of warping warping theory discussed to make the paper self explanatory. The method focuses on how the feasibility is analysed, discussing the geometric properties, boundary conditions and models used. The results show a comparison between the models and experiments, after which a more in-depth characterization is done in ANSYS with a shell model. The discussion and conclusion review the obtained results, its interpretation and future implication.

# Warping in thin-walled structures for differential mechanism applications

Maurice C. Valentijn, Ali Amoozandeh, Giuseppe Radaelli, Just Herder  
Dept. of Precision and Microsystems Engineering  
Delft university of Technology  
Delft, 2628 CD, The Netherlands  
M.C.Valentijn@student.tudelft.nl

*In this paper, the effect of warping in thin-walled beams under torsion is used to create a compliant differential mechanism. This normally negated deformation of the cross section can be used to create an inverse transmission mechanism, resulting in a monolithic and simple alternative without frictional losses and no backlash. This paper presents the characterization of such a beam differential mechanism and determines the influence of the geometric properties on the behaviour. The behaviour is characterized for two functionalities, the geometric advantage of the inverse transmission and the rotational compliance under torque. The simulations are run in finite element software and verified by experiments and analytical calculations.*

*The results show that the torsion constant and warping constant are the geometric properties of influence on the behaviour, where an increase in the warping constant results in an increase in geometric advantage and a reduction of the compliance. An increase in torsion constant results in a minor decrease of the geometric advantage and an almost one on one increase in the stored energy. The model overestimates the geometric advantage by 25% on average and underestimates the compliance of the more stiffer beams with respect to the experiments. The overall conclusion can be drawn that this new kind of differential mechanism has a lot of potential and could certainly serve as an alternative for the classic mechanism.*

## Nomenclature

J	Torsional constant
B	Bimoment
$e$	Shear center
$w$	Warping displacement
$\theta$	Angle of twist per unit length
A	Cross sectional area
$I_w$	Warping constant
E	Young's modulus
G	Shear modulus
$\phi$	Angle of twist
c	Torsional bending constant

## 1 Introduction

Classical thin-walled beams are designed to negate warping, the out-of-plane deformation of the cross section (CS) under torsional loading of a non-cylindrical beam. But, apart from airplane wing adjustment [1], no research has been found into warping beams as a differential mechanism. An intriguing observation, as warping in beams would lend itself to a differential mechanism functionality due to its inverse transmission characteristic during twist. Therefore, this paper aims to further investigate the possibility of using warping to create a differential mechanism from a thin-walled beam.

This warping beam is classified as a compliant shell mechanism. Compliant shell mechanisms are a relative new addition to the field of compliant mechanisms and have been defined as "spatially curved thin walled structures able to transfer or transit force, motion or energy through elastic deformation" by Nijssen [2]. Research has been done into compliant shells for translational transmissions [3], but no rotational transmission or differential related research has been found.

Using a compliant shell as differential mechanisms reduces the number of parts of an assembly, allowing for a monolithic and simple design. The utilization of a compliant shell mechanism will result in a decrease in weight, no backlash, no friction, a less complex design and a prospect for low maintenance [4]. This will make the warping beam differential mechanism suitable for environments like offshore, space or medical as they would benefit from monolithic designs, solving weight or contamination problems. Passive exoskeletons would also benefit from such a light weight solution due to the inherent inverse transmission Degree of Freedom (DoF) during twist, mimicking walking.

The objective of this paper is to show that warping in a beam can be used to create a suitable alternative for the classical differential mechanism. To show that warping can be used to create a differential mechanism, this paper characterizes the behaviour of the warping beam differential mechanism for different geometric properties. The variation of geometric properties are applied to the standard I-,C-, and

Z-profiles. The investigated structures are referred to as "beams", as they are extrusion profiles with a constant CS. Models are used to obtain the results, while experiments and analytical formulas are used to verify the model and chosen geometric properties.

An overview of the theory on warping is given in Section 2 to show how an inverse transmission can be created from a warping beam, select the important geometric properties and give the analytical formulas to compare with the experiments. Section 3 shows the used beams for the experiments, the considered boundary condition, the material choices and the experimental setup. It also presents the models used in the finite element program ANSYS APDL, later referred to as "ANSYS". Section 4 contains the comparison of analytical and finite element models with the experimental results. Section 4 also shows the contour plots made to characterize the beam functionalities over a range of geometric property values. Last, a discussion on the results and a conclusion is given in Section 5 and 6 respectively.

## 2 Theory on warping

If a beam is loaded by uniform or St.Venant torsion, only shear stresses will be present in the cross section. If a cylindrical beam is considered, the shear stresses will be equal throughout the section. Thus, the CS will stay planar and the polar moment of inertia is used to calculate the resulting twist [5]. For non-symmetric beams however, this assumption of a planar CS does not hold anymore, as the shear stresses are not equally distributed, and the resistance is given by the St.Venant torsion constant  $J$  [6].

The shear stresses in these non-symmetrical beams induce a shear strain between the different sections, causing the center elements B and C of Figure 1 to deform. The outer elements A and D do not develop these shear stresses and therefore rotate out of plane, called warping. As stated by Vlasov [7], "The distortion of the plane section caused by longitudinal displacements of its points is called 'The Warping' of a section". Such a case of uniform torsion is illustrated in Figure 2.

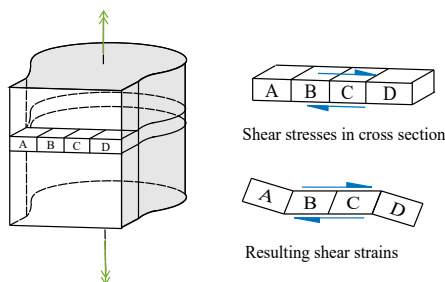


Fig. 1: Visualization of warping in a non-cylindrical beam. The applied torque creates shear stresses in the cross section, causing shear strain, resulting in warping. Adapted from Oden and Ripperger (1981) [5].



Fig. 2: Uniform torsion of a non-cylindrical beam under torsional load.

This out-of-plane deformation of the outer elements is used to create the inverse transmission needed to create a differential mechanism. If the center elements B and C are fixed in space and a single rotation input is given, an out-of-plane displacement of element A and D can still be seen. This displacement of the outer elements will perpetuate through the beam and result in a rotation opposite to the direction of the input rotation, creating an inverse transmission mechanism. However, this is no longer true when warping is constrained.

When warping is constrained, it is called warping or non-uniform torsion [6, 8], after the torsion theory of Vlasov and shown in Figure 3. In this case the theory of St.Venant does not hold anymore and the beam carries load by additional normal stresses [5, 9]. These normal stresses are determined by a generalised force system called the bimoment [7], increasing the torsional stiffness of the beam.

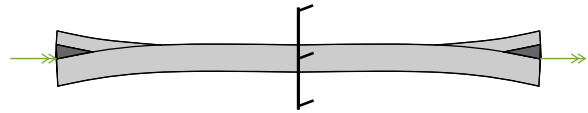


Fig. 3: Non-Uniform torsion of a beam under torsional load.

The bimoment is defined as the bending moment  $M$  multiplied by the CS height  $h$  [9], as visualized for an I-beam in Figure 4a and b. The center piece of the beam section is called the web and the two outer parts are called the flanges. The height refers to the web and the width to the flanges.

The warping moment is the resultant bending moment acting on both flanges, which acts self balancing as the moments are equal in magnitude with opposite direction. The bimoment can not be directly measured and decreases as the distance to the application point of torsion increases. Both the shear stresses and the normal stresses corresponding to the bimoment and bending moments can be seen in Figure 4c.

The resultant twist for both uniform and non-uniform torsion is around the shear center  $e$ . This geometric property is defined as "the point in the plane of the cross section about which twisting takes place" [6]. For an I-beam, the shear center is located at the center web, but for a C-beam it is located outside of the cross section of the beam.

### 2.1 Warping displacement

The warping displacement  $w$  is defined as the out-of-plane displacement of the CS for both uniform and non-uniform torsion. Figure 5 depicts a random cross section, with a piece of the CS called  $ds$ .  $ds$  is defined by the perpendicular distance  $r$  to the defined center point, taken to be the

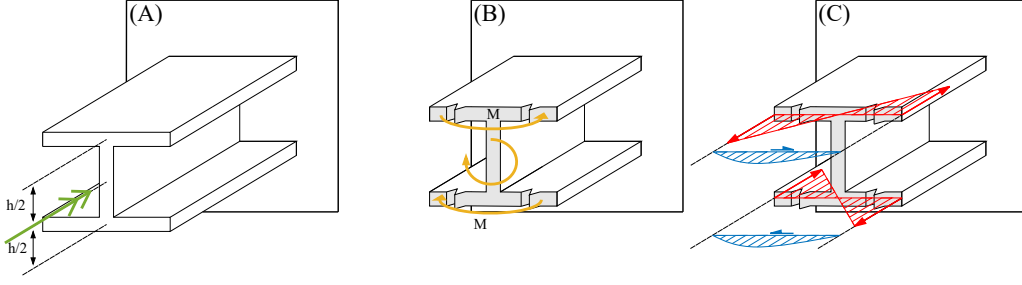


Fig. 4: (a) shows the applied torsion, (b) the resulting moments in the section and (c) the corresponding stresses.

shear center  $e$ , and distance  $s$  from the defined origin of the section.  $\theta$  is defined as the angle of twist per unit length of the whole beam around the  $x$ -axis.

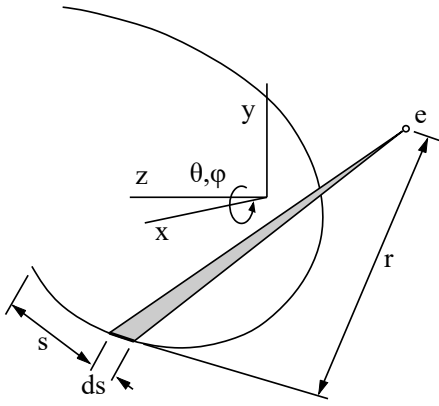


Fig. 5: Parameters used to determine the warping displacement. The shown illustration is all in plane. Illustration adapted from Timoshenko [10].

$$\begin{aligned}
 w &= \theta (\bar{\omega}_s - \omega_s) \\
 \omega_s &= \int_0^s r ds \\
 \bar{\omega}_s &= \frac{1}{A} \int_0^A \omega_s ds
 \end{aligned} \tag{1}$$

The warping displacement is given by Equation 1 [5, 10], with  $A$  being the cross sectional area and  $\omega_s$  the so called warping function, defined as the double sectorial area encompassing the center line  $s$  of the CS.  $\bar{\omega}_s$  is the average warping displacement, a factor used to compensate for the distance between the defined center point and the shear center  $e$ .

## 2.2 Warping constant

The warping constant  $I_w$  is a cross-sectional property and "a measure for the effort needed to reduce warping" with units  $m^6$  [9].

$$I_w = \int_0^A (\bar{\omega}_s - \omega_s)^2 t ds \tag{2}$$

The warping stiffness, or warping rigidity, of a beam is given by multiplication with the Young's modulus ( $E$ ) and is thereby given by  $EI_w$ . This is in line with the notation for torsional stiffness given by  $GJ$ , with  $G$  being the shear modulus and  $J$  the torsional constant.

Similar to completely cylindrical cross sections, cross sections consisting of thin rectangular elements intersecting at one common point do not experience warping either [10], as this will cause the distance  $r$ , shown in Figure 5, to reduce to zero. These type of sections not experiencing warping include V, T and L cross section shapes.

$$\begin{aligned}
 B &= -EI_w \phi'' \\
 T_{tot} &= T_{St.Venant} + T_{Warping} \\
 &= GJ \phi' - EI_w \phi'''
 \end{aligned} \tag{3}$$

Equation 3 shows the equation for the earlier mentioned bimoment, composed of the warping stiffness multiplied by the second derivative of the twist of the beam [5, 7, 10, 11]. The total torsion formula is also given by Equation 3, split up into St.Venant and warping torsion. With  $\phi$  defined as the angle of twist.

$$\phi = A_0 + A_2 e^{cx} + A_3 e^{-cx} + \frac{Tx}{GJ} \tag{4}$$

For a beam under non-uniform torsion with one free and one fixed end, the general solution for the twist of a beam is given by Equation 4, with  $x$  defined as the length along the beam, as shown in Figure 5. With  $c$  being the torsional bending constant [12], defined as  $c = \sqrt{GJ/EI_w}$ . The considered loading case must furthermore adhere to the following boundary conditions:

$$\phi = \frac{d\phi}{dx} = 0 \quad \text{at } x = 0 \quad \text{and} \quad \frac{d^2\phi}{dx^2} = 0 \quad \text{at } x = L$$

$x=0$  is a fixed end and  $x=L$  is a free end. An illustration of the considered problem is seen in Figure 4a. These boundary conditions are given as they are later used in the comparison between the experimental and simulation data.

### 3 Method

In order to establish the characterization of the geometric properties, later compared to the outcome of the experiments and analytical calculations, two ANSYS models are used. First, the different beams are tested in the experimental setup and compared to the ANSYS beam and shell model and the analytical calculations. This verification serves multiple purposes, as the model results and the influence of both the geometric properties and CS shapes are verified.

The torsional constant  $J$  and warping constant  $I_w$  are identified as the two main factors to influence the beam behaviour for both uniform and non-uniform torsion. The shape of the CS is also a variable to be analysed, defined by the shape of the cross section center lines. The shear center  $e$  is not considered as a separate factor as it is included in the definition of warping constant.

The characterization for the geometric properties and different cross sections shapes is split up into two differential mechanism functionalities, these functionalities are investigated using two different load cases. Load case 1 (LC1) is the determination of the geometric advantage of the inverse transmission mechanism, highlighting the internal DoF caused by warping. Load case 2 (LC2) is an applied pure torque to determine the rotational compliance. Furthermore, although compliant mechanisms do not suffer from friction losses, energy is stored in the deformation. Therefore, the energy stored within the beam for LC1 is also shown to determine the energy needed for operation. The analytical formulas are only used to compare to LC2, as no boundary conditions are found for the analytical model of LC1.

#### 3.1 Beam specifications for experiments

Four chosen beam cross sections with varying CS and dimensions are compared to show the effect of  $I_w$ , the type of CS and the validity of the models. Table 1 shows the cross sections of beams to be tested including dimensions and geometric properties.

Beam I1 and I2 have a comparable torsion constant. This way, the effect of the warping constant on both load cases can be shown. The dimensions of beam I1 and C are chosen to have similar  $J$  and  $I_w$ , in order to compare the influence of the CS shape. The same reasoning is behind the comparison between beam I2 and Z. The small deviations in geometric properties for the different torsion constants, warping constants and the cross sectional areas are due to fabrication.

#### 3.2 Boundary conditions for 2 load cases

LC1 is depicted in Figure 6 and is used to determine the geometric advantage of the beam. The output over the input angle is called the geometric advantage and is given within a range from 0 to 1, with 1 being the theoretical maximum in which case the output angle is equal to the input angle. The beam will behave as an inverse transmission as the center web is fixed. Both the input and output angle are measured at the two outer webs. This geometric advantage deviates from a standard differential, mostly used to transmit power.

Table 1: Dimensions and geometric properties of the beams used during the experiments.

Beam name	I1	I2	C	Z
Illustration				
Height [m]	50.75e-3	51.2e-3	50e-3	49.7e-3
Width [m]	45.6e-3	18.9e-3	40.5e-3	13.6e-3
Thickness [m]	0.75e-3	0.82e-3	0.78e-3	0.95e-3
$J$ [m <sup>4</sup> ]	2.0e-11	1.64e-11	2.07e-11	2.2e-11
$I_w$ [m <sup>6</sup> ]	7.63e-12	6.05e-13	8.16e-12	7.23e-13
$A$ [m <sup>2</sup> ]	1.07e-4	7.30e-5	1.022e-4	7.31e-5

LC2 concerns the unconstrained rotational stiffness of each beam as the applied pure torque induces a rotation. This rotation is divided by the input torque and presented as the compliance of the beam, shown in radians per Nm. LC2 applies a torque to the center web, with the outer webs being constrained in rotation around the axis along the beam, as shown in Figure 7.

These two factors are used to gauge the behaviour of the warping beam differential mechanism. A parallel with a conventional differential mechanism can also be drawn for LC2, as the applied torque is equally distributed to both ends.

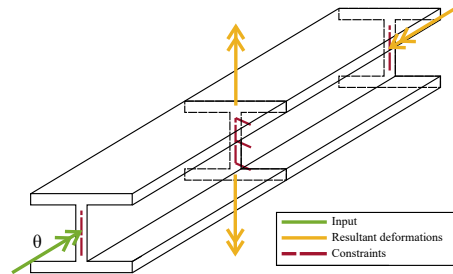


Fig. 6: LC1 considered for the warping beam differential mechanism.

The applied rotational input for LC1 is set at  $45^\circ$  and the applied torque for LC2 is  $0.4Nm$ . A pure rotation and pure torsion are used relatively, so no combined loading is considered. The analysed beams have a length of 360mm, with the CS dimensions being uniform over the length and the position of the constraint at half length.

The webs are constrained as shown in Figure 6 and 7, with the two outer webs constrained with a rigid link. 80% of the web length is constrained to better compare to the experimental setup. A 100% constraint of the web is not chosen as it can not be guaranteed if a clamping method is used to achieve the constraint. The center web is constrained dependent on each of the two load cases, with the flanges being free for LC1 and fixed for LC2.

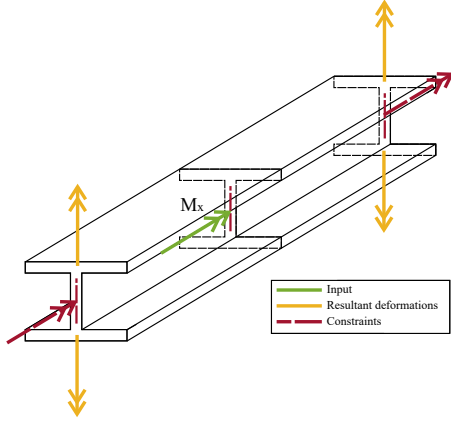


Fig. 7: LC2 considered for the warping beam differential mechanism.

### 3.3 Models and experiment

The material used in both ANSYS and the experiments is polyamide 12 (PA12). The material properties are shown in Table 2, with the tested beams 3D printed using Multi Jet Fusion (MJF). PA12 was chosen to have monolithic test parts, eliminating the effect of added stiffness caused by connection pieces. The material is furthermore assumed to be homogeneous, isotropic and linear elastic.

Table 2: Material properties of Polyamide 12.

$\rho$	$\nu$	E	G	$\sigma_y$
$[kg/m^3]$	$[-]$	$[GPa]$	$[GPa]$	$[MPa]$
1010	0.41	1.2	0.43	38

#### 3.3.1 Ansys models

ANSYS is used to implement warping and make use of the nonlinear geometry for the analysed models. Two models are used in ANSYS, a beam and shell model. Both models are chosen to compare results and decide on the best kind of model to use for such an application.

The beam element used is "BEAM188", suitable for slender beams and based on Timoshenko beam theory, with an additional DoF [13]. The extra DoF gives every node a 7<sup>th</sup> DoF to allow for out of plane displacement. The beam model does not allow an input rotation or torque to be applied to only the web, so an input over the whole CS is used instead. No buckling of the flanges can occur as the projection of the CS on its plane stays undeformed [13].

The "SHELL181" element is used for the shell model as it is well-suited for thin shell structures and large rotations applications. The SHELL181 is made up of four-node elements each having six DoF and is based on the Reissner-Mindlin shell element [14]. For the simulations done with the shell model, the input rigid links and constraints are ap-

plied at the web and thereby better represent the constraints used in the experiment.

#### 3.3.2 Experimental setup

The experimental setup is used to verify the results obtained from ANSYS and show if the predicted influence of the warping constant and CS type is correct. The constraints used for the experiments differ from those used in the simulation as it is a line constraint, so an alternative constraint is used. All three web constraints are applied by clamping the evaluated beam over a width of 3mm. A comparison between the two clamping methods is shown in Figure 8.

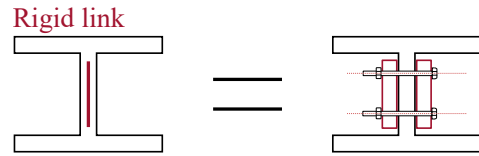


Fig. 8: A comparison between the model constraint, a line contact, and the experimental constraint, a line clamping over a width of 3mm.

For LC1, a pure rotation around the x-axis is created and transferred to the tested beam by a misalignment coupling to allow for movement of the input link, seen in Figure 9. The coupling part couples the rotation to the beam by a rigid link at the web. The inclinometer measures the input angle, also shown in Figure 9. Figure 10 shows the output angle inclinometer supported by a ball support to support its weight. An overview of the constrained beam, the input and output can be seen in Figure 11a. Both inclinometers have a minimal tolerance of  $160^\circ/800$ .

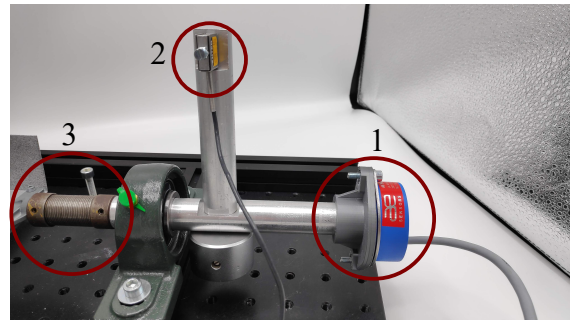


Fig. 9: Side view of the input side of the experiment for LC1. (1) is the input inclinometer, (2) the load cell and (3) the misalignment coupling and connection piece.

For LC2 only half of the beam is tested. A change in constraint is necessary to create the same boundary condition compared to a symmetric load case. This constraint is shown in Figure 12 and is needed as a single input torque instead of a symmetric one is used. The input torque is created

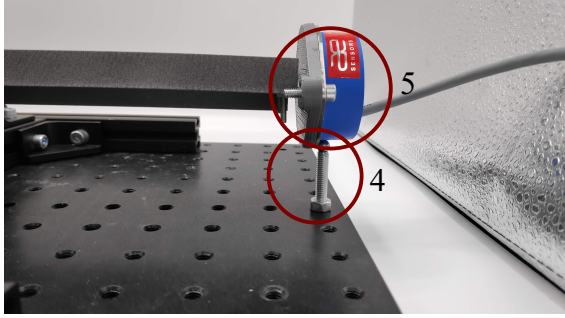
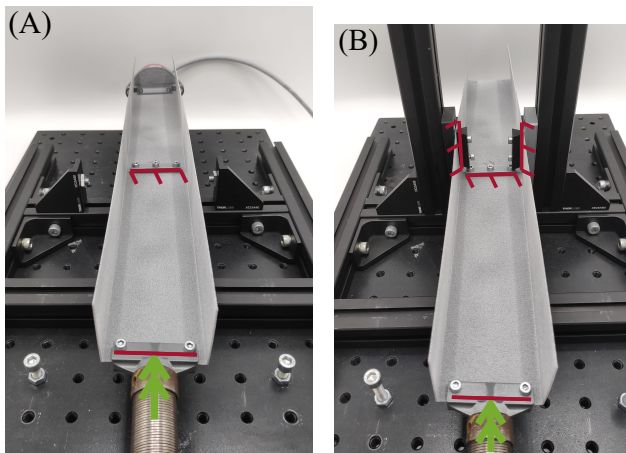


Fig. 10: Side view of the output side of the experiment for LC1. (4) is the ball contact to compensate for the weight of the inclinometer and (5) the output inclinometer.

by the balanced lever seen in Figure 9. The load cell is used to measure the applied pure torsion and the input inclinometer is used to measure the resulting rotation. An overview of the clamped beam for LC2 can be seen in Figure 11b. The load cell has a minimal tolerance of  $9N/1000$  at a distance of  $100mm$ . Thus, the tolerance on the torque is approximately  $0.001Nm$ . The experiment setup for LC2 can be seen in Figure 11b.



(a) The experimental setup for LC1, shown for a C beam. (b) The experimental setup for LC2, shown for a C beam.

Fig. 11: The experimental setup for LC1 and LC2.

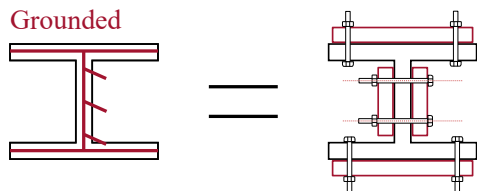


Fig. 12: Experiment constraints for LC2. Instead of the model constraint, a total constraint is created at the center flange.

### 3.3.3 Influence of the torsion and warping constant

After the experiment comparison and verification, only the SHELL181 model is used to characterize the geometric advantage and rotational compliance over a range of cross section dimensions. The shell model is used as its constraints better represent the constraints used in the experiments.

The dimension of the cross sections are varied within a range of dimensions. The maximum design area is set at  $50 \times 50mm$  and the maximum cross sectional area is  $1e^{-4}m^2$ . The width, height and thickness are varied within these bounds to create a multitude of  $J$  and  $I_w$  combinations per CS. Each different combination of dimensions is a datapoint to be run in ANSYS, with the geometric advantage and energy storage for LC1 and the compliance of LC2 computed for each datapoint. The upper and lower bounds of the dimension are set as:

$$\begin{aligned} h_{min}, h_{max} &= [10e-3, 50e-3] \\ w_{min}, w_{max} &= [10e-3, 50e-3] \\ t_{min}, t_{max} &= [0.5e-3, 2e-3] \end{aligned}$$

with  $h$  being the height of the web,  $w$  the width of the flanges and  $t$  the uniform thickness over the web and flanges. The Z CS has a maximum width of  $25mm$  as the flange width is measured from the center of the web.

## 4 Results

The results are shown between the experimental data, analytical formulas and the ANSYS models first. Next, the characterization of both load cases with respect to the torsion and warping constant is shown.

### 4.1 Experiment comparison

One specimen per beam is tested in 2 different orientations in both directions, twice. So 8 sets of data are obtained for each tested beam. For the comparison of the experimental data with the models, every shown data point is an average of the data around  $45^\circ$  and  $0.2Nm$ . For LC1, the data between  $44.5^\circ$  and  $45.5^\circ$  is picked and for LC2 the data between  $0.195Nm$  and  $0.205Nm$ . This is done to minimize the effect of data scatter.

A distinction is made between two rotation directions for the comparison between the experiments and model data. This distinction is made as the Z beam is sensitive to the rotation direction, with the directions as depicted in Figure 13.

Figure 14 shows the results obtained for LC1, showing the 8 different data points obtained for each tested beam and the beam and shell model simulation. The average of the 8 data points is also plotted. The x-axis shows the 4 separate columns for the 4 tested cross sections. The values of both models as well as the averages of the experiments are also given in Table 3.

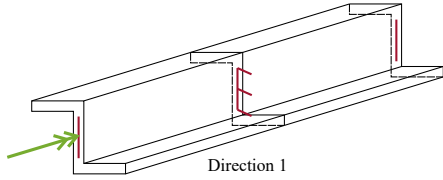


Fig. 13: Rotation direction 1 with respect to tested beams. Direction 2 is opposite to direction 1. The directions are the same between the two different load cases.

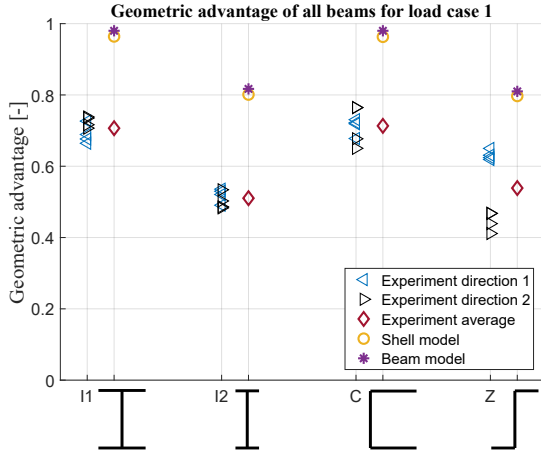


Fig. 14: The compared results for LC1. The average of the 8 data points and the results of the ANSYS beam and shell model are shown. The x-axis shows the 4 different tested beams.

Table 3: The values of the experimental, beam and shell model for LC1.

	I1	I2	C	Z
Beam model	0.98	0.83	0.98	0.81
Shell model	0.96	0.81	0.96	0.80
Experiment average	0.71	0.51	0.71	0.54

As can be seen in Figure 14 and table 3, a maximum difference of 3% for the geometric advantage between the beam and shell model can be seen, with the shell model having a lower overall geometric advantage. The spread between the two specified rotation directions is largest for the Z beam.

The results of LC2 are shown in Figure 15, including the analytical solution based on the boundary condition given in Section 2. A maximum deviation of 50% between the beam and shell model can be seen. Again, the biggest spread between the two directions is seen for the Z beam. Table 4 shows the values for the two models, the result of the analytical calculations as well as the average of all data points.

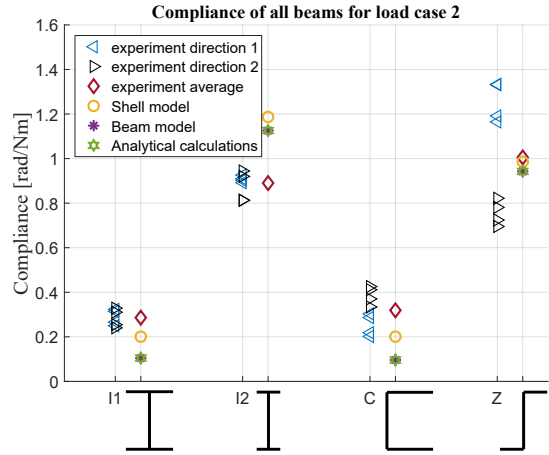


Fig. 15: The compared results for LC2. The average of the 8 data points, the analytical results and the results of the ANSYS beam and shell model are shown. The x-axis shows the 4 different tested beams.

Table 4: The values of the experimental, analytical calculations, beam and shell model for LC1.

	I1	I2	C	Z
Beam model	0.105	1.126	0.096	0.943
Shell model	0.207	1.187	0.207	0.986
Analytical calculations	0.105	1.126	0.096	0.943
Experiment average	0.286	0.890	0.319	1.005

## 4.2 Influence of the torsion and warping constant

The results of the characterization are only performed using the SHELL181 model within ANSYS APDL. The data shown in the following figures is linearly interpolated between the datapoints gathered, with the datapoints depicted by the black dots. No distinction is made between the cross sections for LC1 as the data is equal for all. The data for LC2 is CS dependent for the lower regions of the torsion and warping constant and therefore only the data for the C section is shown.

Figure 16 shows the geometric advantage obtained for a range of both  $J$  and  $I_w$  in a contour plot, with the contour lines depicting the lines of constant value. The yellow is seen as the optimum part as a high transfer of rotation would be preferable. It can be seen that both the torsional and warping constant have an effect on the measured geometric advantage, with Figure 17 depicting the energy stored in the beam corresponding to LC1. A higher energy storage for LC1 is seen as less desirable as it increases the operating energy. These datapoints are calculated by varying the cross sectional dimensions, so not all combinations of torsion and warping constant are obtainable.

Figure 18 shows the compliance for beam C under an applied torque for LC2 for the same datapoints as LC1. It

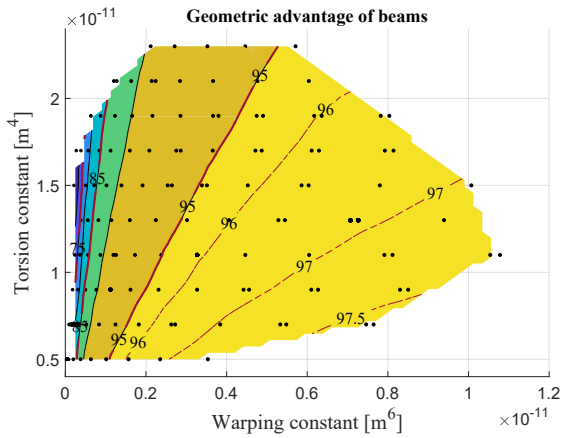


Fig. 16: The geometric advantage of all analysed beams. The contour lines depict constant values throughout the plot and the black dots depict the simulated datapoints.

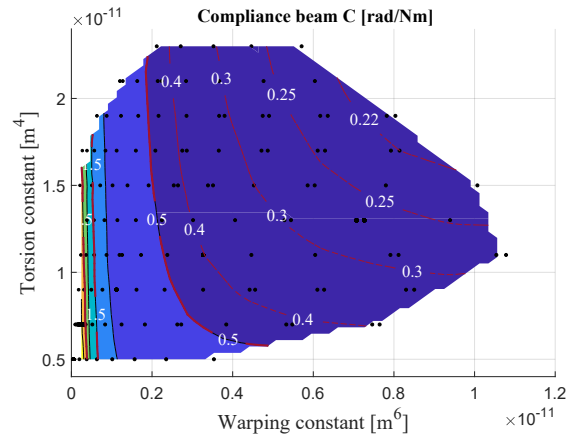


Fig. 18: The rotational compliance of all analysed beams. The contour lines depict constant values throughout the plot and the black dots depict the simulated datapoints.

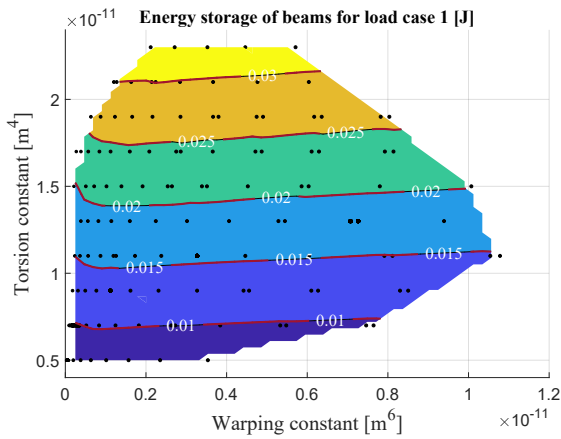


Fig. 17: The energy in the analysed beams under LC1. The contour lines depict constant values throughout the plot and the black dots depict the simulated datapoints.

can be seen that for a larger warping constant, a lower compliance is measured. The blue areas depict cross sections with a low compliance with respect to the applied torque.

## 5 Discussion

### 5.1 Experiment comparison

A spread within the experimental data can be seen in both Figure 14 and 15, which for the I1, I2 and C beams is minor and explainable by local pre-deformations due to production. Hysteresis or visco-elasticity can also cause a deviation but these quantities are harder to quantify. The Z beam is direction dependent due to buckling occurring on the flanges for "direction 2", as the flanges are compressed in this direction.

For LC1, the shell and beam model follow the same trend. As this load case is almost uniform torsion, no deviations between the beam and shell were expected. The model results of LC2 are however noteworthy, as for the more stiffer

beams I1 and C, a difference between the two models up to a factor two can be seen. This is caused by the beam model having a cross section unable to deform. Buckling is seen for both the shell model analysis and the experiments, but not for the beam model. A smaller deviation between the models can be seen for the less stiff beams, as buckling is less prevalent for structures with smaller flanges.

Comparing the model with the experimental results, a loss of 25 to 30% in the geometric advantage can be seen. The experiment center constraint was thought to be of great influence on the transfer of warping through the beam. As the beam is clamped over a length of 3mm, stiffness is created opposing the transfer of warping. This can not occur in the models, as a center web is constraint by a line constraint. Running the shell model with the exact same constraints only, however, results in minor losses with respect to the original results. A fluctuation in cross section thickness can be a more influential factor as the peak thicknesses vary 10% with respect to the mean dimension.

For LC2, the beam model data and analytical calculations are the same, as expected. Both methods assume a static CS with a uniform torsion applied over the whole plane. The shell model deviates from the other two, mainly for beam I2 and Z. A reasoning can be found in a relative rotation observed in the shell model and the experiments between the flanges and the web, not considered for the beam model and analytical calculations.

An underestimation of the real compliance under torque loading of the model can be caused by slight play in both end-constraints. It is however curious to see a constant overestimation of beam I2 under torque loading, for which no explanation is found.

General losses also exist in the setup, affecting both LC1 and LC2. The input and output constraint shorten the beam as a part of the beam is clamped, shortening the effective length. A shorter beam does not necessarily have a lower geometric advantage, so possibly induced stresses over the clamped area can also obstruct the transfer of warp-

ing through the beam. Friction in the ball support can also induce losses relative to both models, just as rotation losses in the misalignment coupling.

## 5.2 Influence of torsion and warping constant

Concluding from Figure 16 and 18, both the warping and torsion stiffness influence the behaviour of the beam. An increase in the warping constant results in both a higher geometric advantage and a higher torsional stiffness. An expected result, as the warping constant can be seen as the resistance against warping torsion [6]. A higher torsion constant results in a slight increase torsional stiffness, and a lower geometric advantage. The energy level of LC1, shown in Figure 17, is highly dependent on the torsional stiffness. As the energy storage is increased by an increase in torsion constant, an expected decrease for the geometric advantage occurred.

As mentioned in Section 4, the contour plots for LC1 are equal over the three analysed cross sections. For LC2 a difference is seen at low torsion and warping constant values, that can be caused by the shortcomings of the nonlinear geometry analysis in ANSYS or other factors dominating at these high deflections.

It is also important to understand the importance of the center constraint, and particularly the length of web that is constraint. Current comparisons are done with 80% of the web length constraint, but lowering it to 60% would results in a change for LC1 of 0.96 to 0.93. For LC2 the rotation compliance would increase from  $0.064\text{rad}/\text{Nm}$  to  $0.126\text{rad}/\text{Nm}$ . It is thereby advised to constraint the web totally, if possible within the scope of a study or design.

## 5.3 Future work

Only pure rotation and torsion is considered in this research, which can be improved on by considering combined loading, a combination of both bending and rotation moment, to closer resemble an implemented design. The energy storage itself also is an important property of the beam. A possible field of interest is adding pre-stress to the flanges before assembly with the web [15], thereby increasing the geometric advantage. Another field of interest that is not considered, is changing the transmission ratio of the warping beam. The center constraint is now placed on the center web, resulting in a maximum geometric advantage of 1:1, but this distance can be changed.

If a further increase in warping constant is desired, with constant area, other cross sections can be considered. Figure 19 shows beam cross sections with an inherent higher warping constant. These cross sections are however aimed at having a square or round design area, so they are not applicable to every design area.

As a design base, web sections like those of an I-beam coincide with the shear center, thus can only be used to influence the torsion constant. If a high warping constant over area is desired, the perpendicular distance between the flanges and the length of the flange should be maximized within the design area. So an optimized structure, with re-

spect to the warping constant, will look like a long open continuous element as far positioned from the center of the structure as possible.

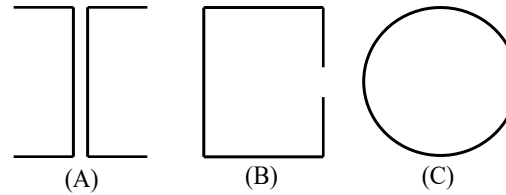


Fig. 19: Possible beam cross sections for future research.

## 6 Conclusion

To conclude, the obtained contour plots can be used to predict the behaviour of standard cross sections for the use as a warping differential mechanism. The maximum theoretical geometric advantage is almost 100%, showing the potential of a warping beam differential mechanism.

The SHELL181 model results are shown to more accurate than the BEAM188 model with respect to the experiments, as the deformation is better captured and the constraints better represent the experimental setup. A large constant over-prediction of 25% is seen for the geometric advantage by both ANSYS models, implying systematic losses. The models have an accurate prediction of the rotational compliance for the more stiffer beams, this accuracy however drops when the less stiffer beams are analysed. With an increase in rotational deformation, the nonlinear material and geometry start to dominate, unable to be captured by the ANSYS model.

The warping constant  $I_w$  can be said to be of large influence on the results of both load cases. The kind of cross section is of less influence, and only needs to be taken into account once buckling of the cross section is expected. The torsion constant  $J$  is shown to have an almost linear relation to the energy stored in the beams for load case 1. A high warping constant over area can be obtained by maximizing the perpendicular distance between the flanges. To tackle the energy stored in the beam during deformation, the torsion constant can be lowered and the maximum warping constant results in the maximum geometric advantage.

Thus, this paper shows that this new kind of differential mechanism, utilizing warping in a thin-walled beam, can be a suitable alternative for a classical one, but a constant offset should be taken into account between the modelled expectations and real functionality.

## References

- [1] R. Vos, Z. Gürdal, and M. Abdalla, "Mechanism for warp-controlled twist of a morphing wing," *Journal of Aircraft*, vol. 47, no. 2, pp. 450–457, 2010.

- [2] J. P. A. Nijssen, "A Type Synthesis Approach to Compliant Shell Mechanisms," tech. rep., Delft University of Technology, Delft, 2016.
- [3] H. W. R. Houwers, "Closed-loop two-fold tape spring transmissions," tech. rep., Delft University of Technology, Delft, 2016.
- [4] L. L. Howell, *Compliant Mechanisms*. New York, USA: John Wiley and Sons, Inc, 2001.
- [5] J. Oden and E. Ripperger, *Mechanics of Elastic Structures*. Washington: Hemisphere Publishing Corporation, second edi ed., 1981.
- [6] Canadian Institute of Steel Construction, "Torsional Section Properties of Steel Shapes," pp. 1–19, 2002.
- [7] V. Vlasov, *Thin-walled Elastic Beams*. Jerusalem: Isreal Program for Scientific Translations, second edi ed., 1961.
- [8] D. Nethercot, P. Salter, and A. Malik, *Design of Members Subject To Combined Bending and Tension*. Berkshire: The Steel Construction Institute, 1989.
- [9] P. C. Hoogenboom and A. Borgart, "Method for including restrained warping in traditional frame analyses," *Heron*, vol. 50, no. 1, pp. 55–68, 2005.
- [10] S. P. Timoshenko and J. M. Gere, *Theory of Elastic Stability*, vol. 29. New York, USA: Mcgraw-hill international book comany, second edi ed., 1962.
- [11] T. V. Galambos, *Structural members & frames*. New York, USA: Dover Publications, Inc, 1996.
- [12] A. F. Hughes, D. C. Iles, and A. S. Malik, *Design of Steel Beams in Torsion*. Berkshire: The Steel Construction Institute, 2011.
- [13] ANSYS, "Theory Reference for the Mechanical APDL and Mechanical Applications," *Knowledge Creation Diffusion Utilization*, vol. 3304, no. April, pp. 724–746, 2009.
- [14] T. Nelson and E. Wang, "Reliable FE-Modeling with ANSYS," *International ANSYS conference*, pp. 1–22, 2004.
- [15] X. Lachenal, S. Daynes, and P. M. Weaver, "A non-linear stiffness composite twisting I-beam," *Journal of Intelligent Material Systems and Structures*, vol. 25, no. 6, pp. 744–754, 2014.



# 3

## Additional results

This chapter elaborates on the obtained experimental results, presenting the raw and smoothed data over a range of input rotations and torque. The input rotation relates to load case 1 (LC1), used to determine the geometric advantage. The input torque is varied for load case (LC2), to determine the rotational compliance.

To further elaborate on the feasibility of a warping beam as differential mechanism, the results of the stress analysis, obtained from ANSYS, are shown. All data obtained from ANSYS is run via MATLAB, for which the code can be found in Appendix D. A complete overview of the experiment setup, for both load cases, is described in Appendix C.

### 3.1. Experiment data

The unfiltered data obtained for LC1 is shown in Figures 3.1, 3.2, 3.3 and 3.4. 2 different tests are done for 2 different orientations. Test 1 and 2 are done for the same orientation as are 3 and 4, with the beam rotated around the axis perpendicular to the web between the tests. The data of all four beams shows a convergence of the data at 0 degrees towards infinity and a difference in geometric advantage between the two input rotation directions.

Figure 3.5 shows the averaged and smoothed data obtained for LC1, with the data of every tested beam presented for an input range of 10 to 45 degrees. The minimal shown input rotation is 10 degrees as the data becomes too disturbed at lower input angles and a moving average is used to smoothen out the data. A comparison is made between the smoothed average data and the shell model predictions shown in Figure 3.5. It can be seen that the ANSYS shell model predicts a linear trend for the considered boundary conditions and constraints. It should also be noted that the ANSYS trend for beam I1 and C overlap.

Figures 3.6, 3.7, 3.8 and 3.9 show the unfiltered data obtained for the experiments for load case 2. The compliance shown on the y-axis is defined by the output rotation over the maximum torque of 0.4Nm, to be consistent with the data obtained in Chapter 2. The same test procedure is used for LC1 and LC2, so test 1 and 2 are done in the same orientation. The "loops" shown for all four analysed beams indicate visco-elastic behaviour and hysteresis of the material. A hysteresis loop can be seen for all four tested beams.

Figure 3.10 shows the averaged and smoothed data obtained for LC2. The data is shown between 0.1 and 0.4Nm, as the data below 0.1Nm goes into the negative compliance regime. A comparison is made with the shell model trends obtained from ANSYS, showing a linear gradient for all four considered beams. Again, the ANSYS predictions show an overlap between the I1 and C prediction.

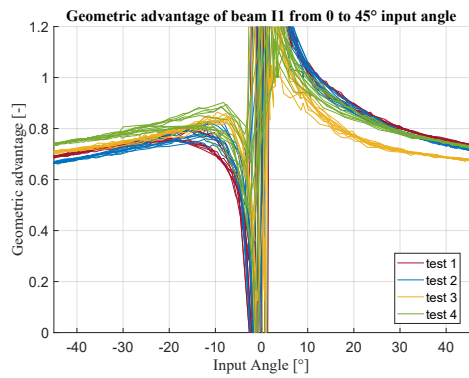


Figure 3.1: The unfiltered experimental data for the geometric advantage, with an input angle of -45 to 45 degrees for beam I1. 4 tests are done per beam, with test 1 and 2 done in the same orientation and 3 and 4 in the other orientation.

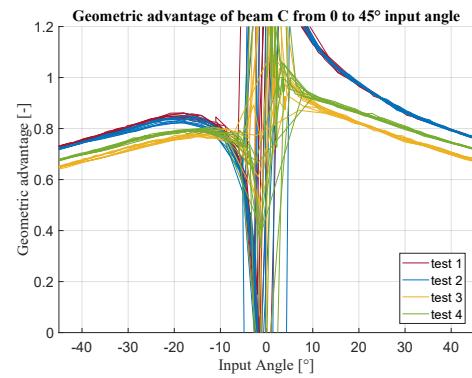


Figure 3.2: The unfiltered experimental data for the geometric advantage, with an input angle of -45 to 45 degrees for beam C. 4 tests are done per beam, with test 1 and 2 done in the same orientation and 3 and 4 in the other orientation.

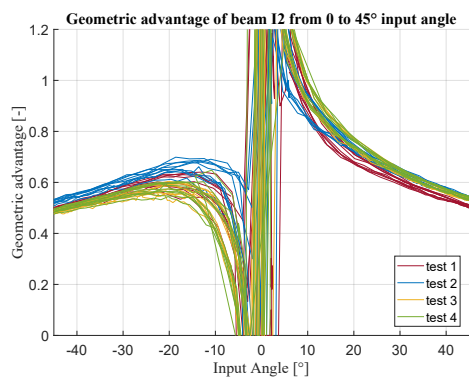


Figure 3.3: The unfiltered experimental data for the geometric advantage, with an input angle of -45 to 45 degrees for beam I2. 4 tests are done per beam, with test 1 and 2 done in the same orientation and 3 and 4 in the other orientation.

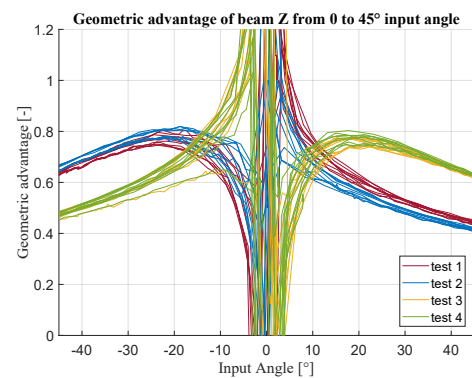


Figure 3.4: The unfiltered experimental data for the geometric advantage, with an input angle of -45 to 45 degrees for beam Z. 4 tests are done per beam, with test 1 and 2 done in the same orientation and 3 and 4 in the other orientation.

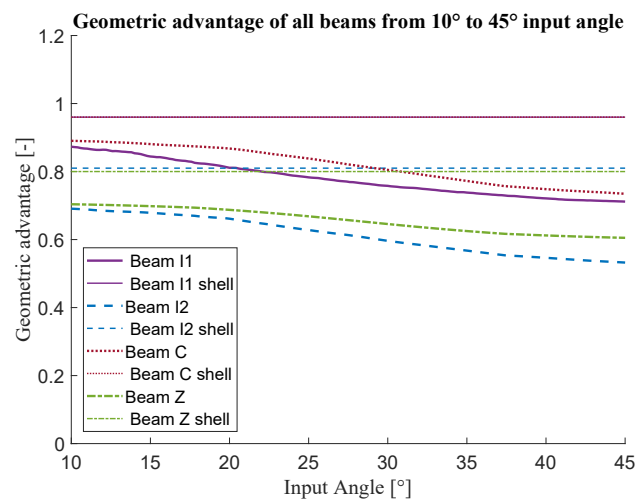


Figure 3.5: The filtered average experimental data and shell model prediction for the geometric advantage, with an input angle of 10 to 45 degrees.

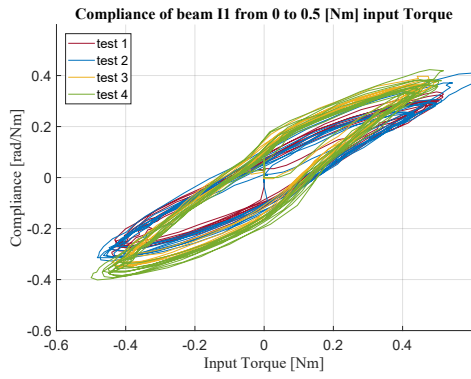


Figure 3.6: The unfiltered experimental data for the rotational compliance, with an input torque of -0.4 to 0.4 Nm for beam I1. 4 tests are done per beam, with test 1 and 2 done in the same orientation and 3 and 4 in the other orientation.

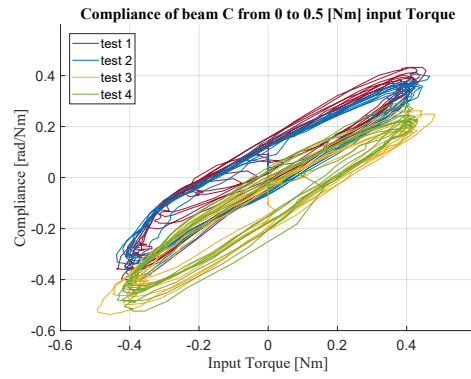


Figure 3.7: The unfiltered experimental data for the rotational compliance, with an input torque of -0.4 to 0.4 Nm for beam C. 4 tests are done per beam, with test 1 and 2 done in the same orientation and 3 and 4 in the other orientation.

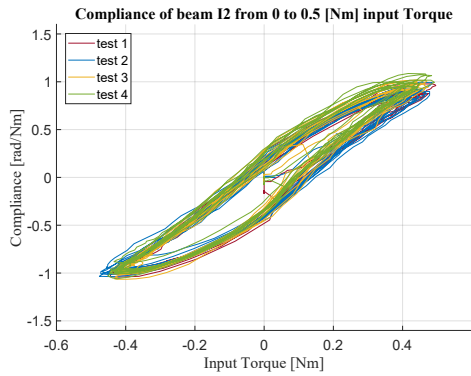


Figure 3.8: The unfiltered experimental data for the rotational compliance, with an input torque of -0.4 to 0.4 Nm for beam I2. 4 tests are done per beam, with test 1 and 2 done in the same orientation and 3 and 4 in the other orientation.

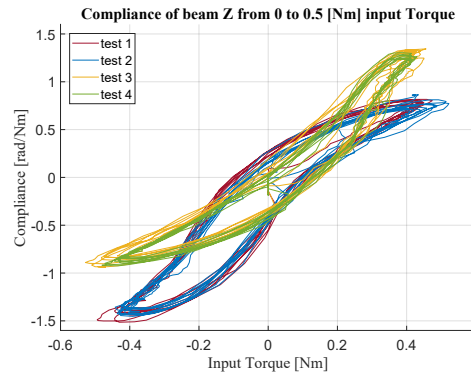


Figure 3.9: The unfiltered experimental data for the rotational compliance, with an input torque of -0.4 to 0.4 Nm for beam Z. 4 tests are done per beam, with test 1 and 2 done in the same orientation and 3 and 4 in the other orientation.

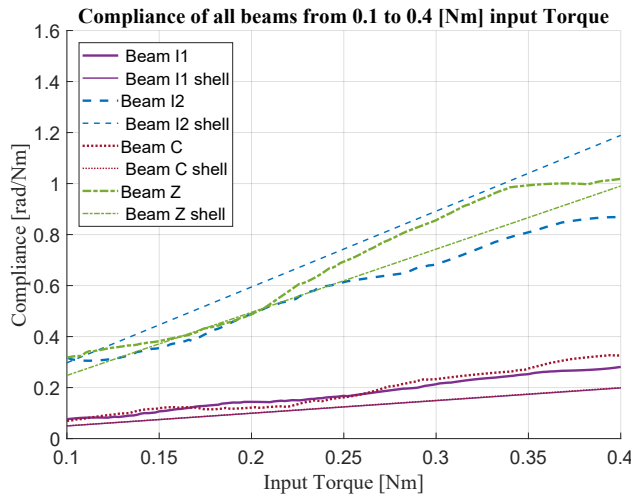


Figure 3.10: The filtered average experimental data and shell model prediction for the rotational compliance, with an input torque of 0.1 to 0.4Nm.

### 3.2. Stress analysis

A stress analysis is done to pinpoint the positions of highest stress. For beam I1, an I-beam with longer flanges, the results of the stress analysis are shown in Figure 3.11 and 3.12 for both LC1 and LC2. For beam I2, an I-beam with small flanges, Figure 3.13 and 3.14 show the deflection and stresses for load case 1 and 2 respectively. Local buckling of the shell flanges can be seen for both beams under LC2.

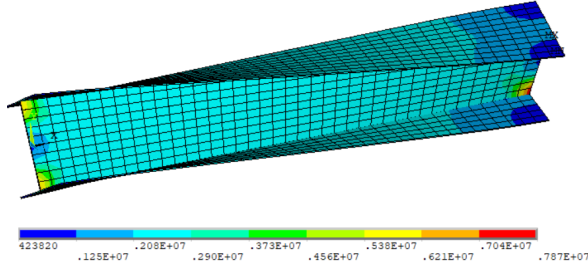


Figure 3.11: Stress analysis of beam I1 for load case 1.

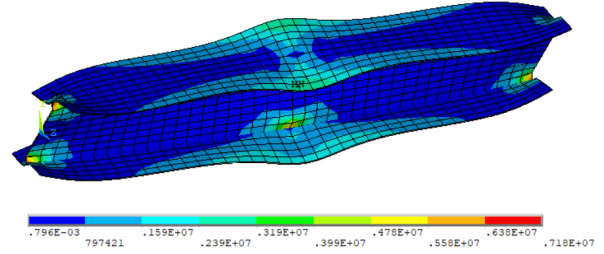


Figure 3.12: Stress analysis of beam I1 for load case 2.

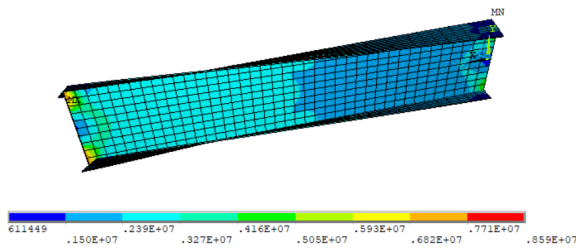


Figure 3.13: Stress analysis of beam I2 for load case 1.

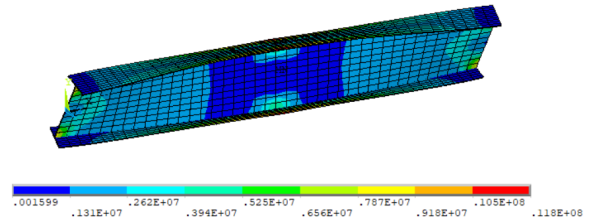


Figure 3.14: Stress analysis of beam I2 for load case 2.

# 4

## Discussion

In this chapter the experimental and smoothed average data of Chapter 3 is reviewed. Furthermore, the data obtained in the ANSYS shell model analysis and the stress analysis is discussed, with the final part of the discussion elaborating on future research.

### 4.1. Experimental data

The convergence of the data towards infinity at 0 degrees input angle for LC1 is caused by pre-deformation of the tested beams and the instability of measuring around zero degrees. The pre-deformation causes a large difference at low input angles between a positive and negative input rotations, with the effect fading away at higher input angles. The convergence of the data towards infinity is caused by the measuring setup, as deviations in the measurements around zero cause the captured data to swing to positive and negative around zero, causing the division of the output angle over the input to result in asymptotic behaviour.

Figure 3.4, depicting the geometric advantage of the Z beam, shows a big difference between the four separate tests due to local shell buckling of the flanges under compression. A positive input angle for test 1 and 2 will result in buckling, thereby lowering the geometric advantage. A negative input angle will not result in buckling, as the flanges are not compressed. The results for test 3 and 4 are vice versa as the tested beam is clamped the other way around.

The smoothed average geometric advantage decreases over the input angle with respect to the linear trend predicted by the ANSYS simulation, both shown in Figure 3.5. This loss in geometric advantage can be caused by imperfections in the experimental setup or material properties of the tested beams. The material properties can be sensitive to hysteresis and visco-elasticity or the dimensions are nonlinear over the width and thickness of the beams. To compensate for this decline in geometric advantage, a more linear material like springsteel or a different production method can be used.

A hysteresis loop can be seen for all four tested beam under LC2, implying that the state of the system is dependent on its history. An offset between the loops can be seen for beam C (Figure 3.7), with test 1 and 2 having a positive offset with respect to test 3 and 4. This behaviour is caused by the pre-deformation of the beam and can also be seen for beam C under LC1 (Figure 3.2). Beam Z again shows the asymmetric buckling (Figure 3.4), also seen for LC1 in Figure 3.4.

Figure 3.10 shows the smoothed average data of the experiments and the ANSYS shell predictions. The shell model predicts a linear trend, also seen for all four tested beams. The stiffer beams I1, C and Z have a slight linear offset but show the same trend, while beam I2 deviates more from the shell model prediction. The I2 beam is the only beam for which the shell model over-predicts the compliance of the beam, as was also seen in Chapter 2, but no explanation is found for this behaviour.

## 4.2. Stress analysis

The stresses for LC1 are seen in Figure 3.11 and 3.13, showing the highest stress concentration at the input constraint as well as at the output constraint. Optimizations of the dimensions can be done to relieve stress, but general stress reduction can be achieved by constraining the total web.

Figure 3.12 and 3.14 show the stress results of LC2. Stress concentrations are again seen at the input and output constraint, but additional high stresses can be seen on the center plane. A difference can be seen between both figures as an increase in flange width implies an increase in stress at this center plane. Local shell buckling can also be seen in both figures, more prominent in beams with larger flanges.

## 4.3. Future work

The steps to be taken after this research can go into two directions, the kinematic functionality can be optimized for design applications or more fundamental research can be done to add functionalities. Before the warping beam differential mechanism can be implemented into a design, it is advised to increase the scope of the characterization by combining the two load cases. Looking at Figure 1.1, this combined load case would involve bending of the torso while having the upper legs in a non zero degree position with respect to the torso. This way of lifting is not uncommon and should be considered if the beam differential mechanism is applied to a passive exoskeleton. Research into the effect non-pure loading has on the characterization is also recommended, as the pure rotation and torque do not totally represent the actual load cases. Investigating the effect of an added bending torque during loading would correspond to the existing way of using the passive exoskeleton.

To add functionalities to the warping differential mechanism, multiple ideas are given. Research into adding a remote center of rotation would let the beam transfer its functionality around bends or around a non-reachable rotation center, which can be used to position the differential mechanism around the hips without adding discomfort. Pre-stressing the flanges before assembly would be another addition to the differential mechanism, as it will add zero-stiffness and multi-stability to the mechanism [10], aiding the walking functionality as no energy is stored while also increasing the geometric advantage.

A possible warping beam differential mechanism is given in Figure 4.1 [19]. To combine the high torsional stiffness with the warping Degree of Freedom, a slid tube with flexures is proposed as a possible solution. This shown example would behave as a cylindrical beam under symmetric loading that would allow for warping to transfer rotation under a non-symmetric loading.

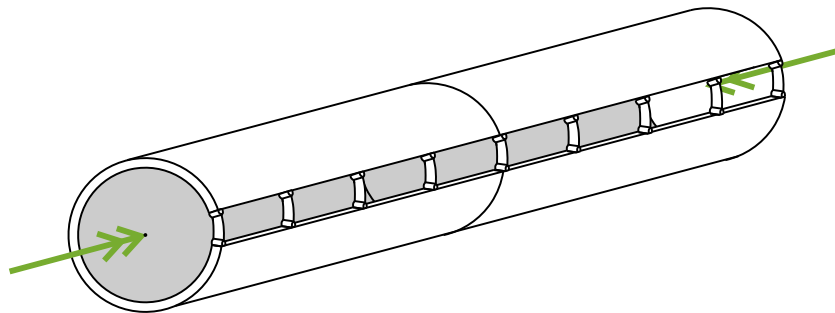


Figure 4.1: Illustration of a possible beam to be used for future research. A slid tube with connecting flexures to allow for warping during non-symmetric loading but stiff under torsion for the shown symmetric load.

# 5

## Conclusion

In this thesis, a new kind of differential mechanism is proposed to add walking functionality to a passive exoskeleton. This new differential mechanism utilizes warping to create the kinematic behaviour of an inverse transmission in a beam. Warping is a normally negated deformation of the cross section, but can be used to create a monolithic and simple solution to the problem posed by a passive exoskeletons.

Research on the potential of such a warping beam differential mechanism is done by characterizing and validating a variation of beam cross sections. The torsion and warping constant are the geometric properties of most influence on the characteristics of the two analysed functionalities, shown by the models and experiments. The warping constant has a large influence on the geometric advantage, the ratio between the out- and input ratio, and the rotational compliance under restrained warping. The torsion constant has less influence on the geometric advantage and torsional stiffness, but scales almost linear with stored energy in the beam. The type of cross section, like C, I or Z, has no influence on the behaviour unless the rotation stiffness is too low and buckling occurs.

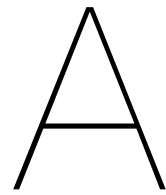
The experiments and analytical calculations are used to validate the model results. The models capture the trends observed by the experiments, but a systematic over-prediction can be seen with respect the experiments. Improvements need to be made to reach the theoretical obtained results but it is shown that a warping beam can be used to create a differential mechanism and a lot of potential is seen in future research.



# Bibliography

- [1] S. J. Baltrusch, J.H. van Dieën, C. A.M. van Bennekom, and H. Houdijk. The effect of a passive trunk exoskeleton on functional performance in healthy individuals. *Applied Ergonomics*, 72:94–106, 2018.
- [2] C. Basaglia, D. Camotim, and N. Silvestre. Torsion warping transmission at thin-walled frame joints: Kinematics, modelling and structural response. *Journal of Constructional Steel Research*, 69(1):39–53, 2012. doi: 10.1016/j.jcsr.2011.07.016.
- [3] Marcelo J. Bianco, Abinet K. Habtemariam, Carsten Könke, and Volkmar Zabel. Analysis of warping and distortion transmission in mixed shell–GBT (generalized beam theory) models. *International Journal of Advanced Structural Engineering*, 11(1):109–126, 2019. doi: 10.1007/s40091-019-0221-9.
- [4] Tim Bosch, Jennifer van Eck, Karlijn Knitel, and Michiel de Looze. The effects of a passive exoskeleton on muscle activity, discomfort and endurance time in forward bending work. *Applied Ergonomics*, 54:212–217, 2016. doi: 10.1016/j.apergo.2015.12.003.
- [5] Canadian Institute of Steel Construction. Torsional Section Properties of Steel Shapes. pages 1–19, 2002.
- [6] Theodore V. Galambos. *Structural members & frames*. Dover Publications, Inc, New York, USA, 1996. ISBN 9780486811840.
- [7] A F Hughes, D C Iles, and A S Malik. *Design of Steel Beams in Torsion*. The Steel Construction Institute, Berkshire, 2011. ISBN 9781859422007.
- [8] IFtoMM. Terminology for the theory of machines and mechanisms. *Mech. Mach. Theory*, 26(5): 435–539, 1991.
- [9] C.F. Kollbrunner and K. Basler. *Torsion in Structures*. Springer-Verlag, Berlin, 1969. ISBN 9783662225592.
- [10] Xavier Lachenal, Stephen Daynes, and Paul M. Weaver. A non-linear stiffness composite twisting I-beam. *Journal of Intelligent Material Systems and Structures*, 25(6):744–754, 2014. ISSN 1045389X. doi: 10.1177/1045389X13502853.
- [11] D.A. Nethercot, P.R. Salter, and A.S. Malik. *Design of Members Subject To Combined Bending and Tension*. The Steel Construction Institute, Berkshire, 1989. doi: 10.14359/11152.
- [12] J P A Nijssen. A Type Synthesis Approach to Compliant Shell Mechanisms. Technical report, Delft University of Technology, Delft, 2016.
- [13] J.T. Oden and E.A. Ripperger. *Mechanics of Elastic Structures*. Hemisphere Publishing Corporation, Washington, second edition, 1981.
- [14] Barre de. Saint-Venant. Memoire sur la torsion des prismes, 1853.
- [15] Shabnam Shayan and K. J.R. Rasmussen. A model for warping transmission through joints of steel frames. *Thin-Walled Structures*, 82:1–12, 2014. doi: 10.1016/j.tws.2014.03.017.
- [16] S. P. Timoshenko and J. M. Gere. *Theory of Elastic Stability*, volume 29. Mcgraw-hill international book company, New York, USA, second edition, 1962. doi: 10.1115/1.3636481.
- [17] Herman van der Kooij. Exoskeleton, 2020. URL <https://www.tudelft.nl/en/3me/about/departments/biomechanical-engineering/research/dbl-delft-biorobotics-lab/exoskeleton/>.

- 
- [18] V. Z. Vlasov. *Thin-walled Elastic Beams*. Isreal Program for Scientific Translations, Jerusalem, second edi edition, 1961.
- [19] Roelof Vos, Zafer Gürdal, and Mostafa Abdalla. Mechanism for warp-controlled twist of a morphing wing. *Journal of Aircraft*, 47(2):450–457, 2010. doi: 10.2514/1.39328.



## Literature study

A literature study is done to collect and generate suitable mechanical topologies to be used in an exoskeleton, to aid the natural walking of the user. An overview of both differential and remote center of rotation mechanisms is made. Suitable combinations are presented to show possible solutions.

PME DEPARTMENT

---

**LITERATURE REPORT: DIFFERENTIAL MECHANISM FOR  
REMOTE CENTER OF ROTATION APPLICATIONS**

---

September 30, 2020

Maurice Valentijn 4387511  
Coaches: Giuseppe Radaelli &  
Ali Amoozandeh Nobaveh  
TU Delft

## Contents

<b>1 Introduction</b>	<b>4</b>
1.1 Motivation . . . . .	4
1.2 Problem statement . . . . .	4
1.3 Report outline . . . . .	6
<b>2 Method</b>	<b>7</b>
2.1 Goal decomposition . . . . .	7
2.2 Characterization . . . . .	7
2.3 Combining features . . . . .	8
<b>3 Literature search</b>	<b>9</b>
<b>4 Results</b>	<b>11</b>
4.1 Topology matrices . . . . .	11
4.1.1 Differential mechanisms . . . . .	11
4.1.2 Remote center of rotation mechanisms . . . . .	11
4.2 Application designs . . . . .	14
<b>5 Discussion</b>	<b>16</b>
5.1 Evaluation . . . . .	16
5.2 Future research . . . . .	16
<b>6 Conclusion</b>	<b>17</b>

## Abstract

The commercial exoskeletons market can be split up into passive and active exoskeletons. Passive exoskeletons are of particular interest as they can aid the functioning of the user without any actuation or power source. Studies have proven that muscle activity can be lowered but to the expense of a higher metabolic rate. The increase in metabolic rate is particularly higher during walking, implying no correct alignment with the body, added weight or added stiffness.

A differential mechanism and remote center of rotation mechanism can be used to aid comfort and ergonomics in these exoskeletons while still aiding lifting. A differential mechanism can combine walking and lifting functionalities and a remote center of rotation mechanism aids the alignment of an exoskeleton with respect to human movement. Topology characterization is done of both mechanisms to find feasible combinations. A literature search is done to find all different topologies, adding them to a ACCREx method inspired matrix. The concluding topologies are used to make a synthesis of various differential and remote center of rotation mechanism, suitable in a passive exoskeleton. The results show the desired functionalities but can have shortcomings like wear and tear. It is thereby advised to investigate compliant subsystems to eliminate the shortcoming of the more classical mechanism investigated.

**keywords:** *Differential mechanism, Remote center of rotation, exoskeleton, topology characterization*

# 1 Introduction

## 1.1 Motivation

With the exoskeleton market evergrowing, comfortability and ergonomics need to be addressed. The exoskeleton market was worth 125 million USD dollars in 2017 and is expected to increase fifteenfold by 2025 [1]. Exoskeletons can be split into two types, active and passive. Active exoskeletons are used to increase the strength of the user or focus on giving back full mobility to paralysed people. Active exoskeletons will not be considered in this report. Passive exoskeletons differ from their active counterpart by not using any external energy to power the exoskeleton, meaning that all power utilized during operation is self-generated. The goal of passive exoskeletons is not to fully take over all the force a human has to exert but instead lowers it. Its application fields are mainly in rehabilitation and industry. Car manufacturers like Ford and Hyundai already utilize exoskeletons to reduce work fatigue for workers working above their head [2, 3].

The focus of this report concerns passive lifting exoskeletons in particular. To have benefit from these passive exoskeletons, they need to be functional and comfortable. It is proven that the Laevo, a passive exoskeleton for lifting, lowers the lower- and upper back muscle activity up to 38% and has a beneficial effect on the metabolic rate of 17% [4, 5]. On the contrast, the Laevo increases the metabolic rate by 12% during walking [5]. There is no record of a passive exoskeleton, that tackles the problem of walking discomfort while aiding lifting. There are however passive exoskeletons that utilize switches, like the Laevo and SuitX. These switches turn the exoskeleton on or off, implying that no real solution has been found for walking without increasing the metabolic rates [6],[7]. To make industry more accessible to adopting exoskeletons, force assistance needs to be enabled without conceding on walking comfort.

## 1.2 Problem statement

To make the challenge at hand more specific, the cause has to be pinpointed. A picture of the Laevo can be seen in figure 1. Both legs contribute to half the force delivered to the chest plate. The force scales w.r.t. the angle between the trunk and leg. This is beneficial during lifting but causes a problem during walking, as the legs do not make a symmetric movement anymore.

This results in a force on the chest and a force on the leg countering the step forward. This system, considering from the waist up, can be seen as a 2 input, 1 output system with 1 Degree of Freedom (DoF), as seen in figure 2. A functionality needs to be added to the exoskeleton such that the two leg forces still add up when making identical movements (as with walking), as they do now, but cancel when the legs counter each others movement. Thus adding a DoF to the system is needed. With the given definition and problem, a differential mechanism poses a solution. According to the IFToMM definitions, a differential mechanism is a "*Mechanism for which the degree of freedom is two and which may accept two inputs to produce one output or may resolve a single input into two outputs*" [8].

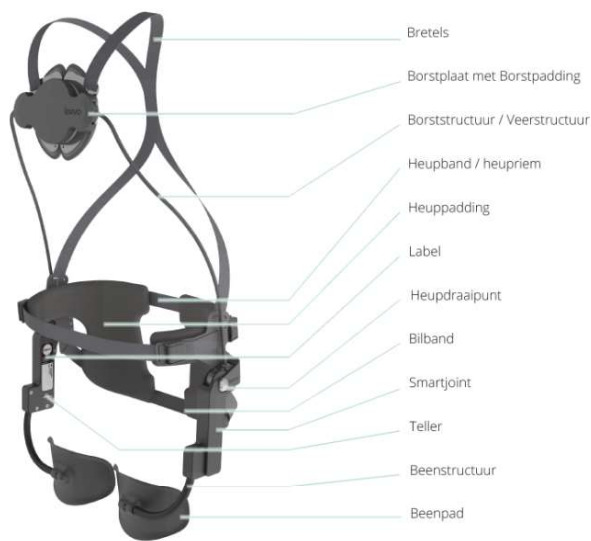


**Figure 1:** Laevo (Intespring, Delft, Netherlands).

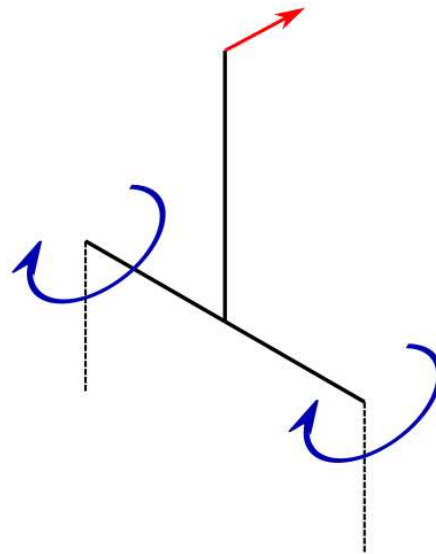


**Figure 2:** Stick illustration of the Laevo passive exoskeleton.

Another feature of exoskeletons that keeps it from moving natural with the body is the positioning of the hinges. The hip mechanism of exoskeleton joints mostly have one out of these 3 topologies, manual alignment, compliant elements or the addition of kinematic redundancy [9]. Manual alignment is labor intensive as everyone is different and bluntly swapping rotational bearing for compliant mechanisms adds to much stiffness. The kinematic redundancy suffers from a high complexity resulting in higher mass systems [9, 10]. Adding compliant mechanisms is not as much used as the other types, so no real results are obtained either. The key within all these possibilities is adding a remote center of rotation, also making it necessary for the differential mechanism.

So to have better comfort in the exoskeleton during walking, 2 features are investigated. The first one being a differential mechanism and the second is the addition of a remote center of rotation hip joint. The goal of this report is to collect and generate suitable mechanical topologies to be used in an exoskeleton to aid the natural walking of the user.

A synthesis of a differential and remote center of rotation mechanisms will be made. The goals can be formulated as followed:

- **Goal 1:** Characterize differential mechanism by their topology.
- **Goal 2:** Characterize remote center of rotation (rcr) mechanisms by their topology.
- **Goal 3:** Find suitable topology combinations to create differential mechanism with a remote center of rotation.

To keep the search and characterization within boundaries, hydraulics and pneumatics will not be considered. Neither will electronic systems, keeping the results are pure mechanical. This is preferred as adding these systems will increase the complexity and lower the robustness. An exoskeleton with either hydraulics, pneumatics or electrical systems will also make the system dependent on outside inputs like electricity or pressured air. Mechanical counterparts of non-mechanical systems will not be excluded. The addition of these systems would make a passive exoskeleton too complex or too bulky.

### **1.3 Report outline**

In section 2, the characterization method is established. The search criteria are determined for the individual searches as well as settings the criteria for the combination stage. Section 3 shows how the searches are performed. Section 4 includes the results and shows the topology matrices. Section 4.2 shows the possible combinations of the 2 independent searches and the discussion and conclusion can be found in Sections 5 and 6.

## 2 Method

This section describes the characterization of the mechanism by first decomposing the problem statements into technical actions. The characterization method is explained, after which the synthesis is elaborated on.

### 2.1 Goal decomposition

As given in section 1, the definition of a differential mechanism is a "*mechanism for which the degree of freedom is two and which may accept two inputs to produce one output or may resolve a single input into two outputs*". Rcr can be split up into planar, spatial or spherical movement, which are defined as:

- **Planar:** *Motion of a rigid body in which its points describe curves located in parallel planes* [8].
- **Spatial:** *Motion of a body in which at least one of its points describes a spatial curve* [8].
- **Spherical:** *Spatial motion of a body in which all points of the body move on concentric spheres* [8].

These definitions can be used to set the frame for the classification of the mechanisms. Such that the differential will be split up into the different in- and output possibilities and the rcr mechanism will be characterized by planar, spatial or spherical orientation. This will also help the literature search as specific words and combinations can be used to fill in the blank spots.

### 2.2 Characterization

The ACCREx method will be used to set a base for the sorting of the different mechanisms [11]. the ACCREx method is a systematic design method which aids the brainstorming by creating a matrix to fill in. Both the columns and rows are defined such that combinations can be searched or self-comprised. This way, no certain topology is left out and a closed "system" is created. This method is normally used to find novelty within a market for a new device or mechanism, for this report its mindset is used to try and make sure that all different topologies are represented.

The differential matrix is sorted with input/output directions on one axis, the transmission input/output on the other axis. Figure 3 shows how the rows and columns are used to make a distinction between the different mechanism that fit into the definitions of a " differential mechanism". As said in section 2.1, the definition will be used to aid the sorting. Both the rows are columns are sorted by methods the mechanism handles and transforms the input.

The rcr matrix columns are sorted by the dimensions in which a rcr mechanism can be accomplished, again making it closed. The rows are chosen to make the rcr matrix better comparable and integrateble into an end-product together with the differential mechanism. A maximum of 3 DoF is chosen as more would not make sense on a hip joint with 3 DoF. The rcr matrix can be seen in figure 4.

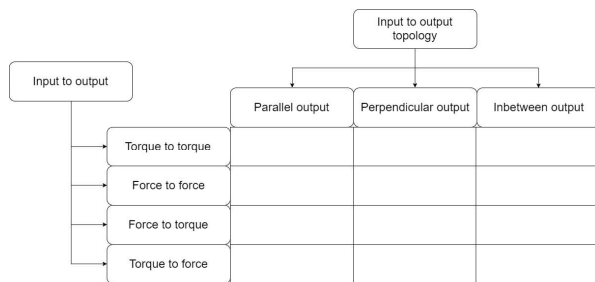


Figure 3: The differential mechanism matrix.

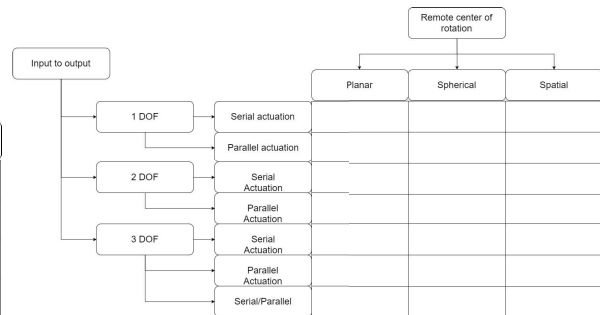


Figure 4: The remote center of rotation matrix.

### 2.3 Combining features

After filling in both matrices, a combination of the two mechanisms needs to be made. This is done finding differential mechanisms with an inherent rcr, and otherwise combining it with a rcr mechanism to create one. The differential mechanisms are chosen by looking at size and input/output direction.

Key features are identified in the designs. To see if they could be applicable, a comparison is made with rating criteria often used for exoskeletons. These criteria are: range of motion, weight, size and DoF [10, 12]. Furthermore, pre-tension and wear are added to this list, as they are important in passive exoskeletons.

### 3 Literature search

This section elaborates on how the results are obtained. The actual results are displayed in section 4. As said in section 2, the definitions are utilized to aid the search. As mentioned in section 1, active systems and fluidics are excluded from the search but passive systems can still be obtained from these search hits. Electronics or other active systems are excluded as the application is for a passive exoskeleton and fluidics are excluded as it adds unnecessary complexity. The literature search is split up into two, both having the same approach but of course differentiating with search terms and results.

Searches were done on Scopus, Google scholar, Google, TU Delft Library catalogus, TU Delft repository and Espacenet. Searches were done in two steps, generic searches and specific searches. Generic searches were used to, next to filling in the matrices, possibly identify missing combinations. If such a missing combination was found, a suitable matrix index followed. The specific search was performed to search for specific combinations to make sure no topology is missed. Table 1 shows the search terms for the Differential mechanisms, table 2 shows those of the rcr searches.

**Table 1:** The search terms used to fill the differential mechanism matrix. The F16H search term is the Cooperative Patent Classification (CPC) for differential mechanisms.

Keywords	Including (AND)	Excluding (NOT)
"differential mechan*"	"mechanical"	
"exoskelet*"	"lifting", "mechanical"	
"exoskelet*"	"lifting", "passive"	"active"
"differential"	"compliant", "mechan*"	"differential equation"
"diffential"	"mechan*", "underactuated"	
"transmission"	"multi input"	
"wippletree"		
"2 input"	"1 output", "mechanism"	
"motion coupling"		
"differential mechanism"	"mechanical"	"vehicle"
F16H		"vehicle"

**Table 2:** The search terms used to fill the remote center of rotation search terms.

Keywords	Including (AND)	Excluding (NOT)
"remote center of rotation"	"mechan*"	"drug"
"remote center of motion"	"mechan*"	"drug"
"spherical"	"mechan*"	
"spatial"	"mechan*", "remote center"	
"curved"	"mechan*", "mechanical"	"reaction"
"spherical scissor"		
"agile eye"		
"shell*"	"deployable", "mechan*"	
"shell*"	"structures", "morphing"	
"shell*"	"compliant"	
"shell*"	"cylindrical", "foldable"	
"remote center"	"mechan*"	

## 4 Results

This section shows the results found in literature. The decision matrices are explained after which possible topologies are shown for exoskeleton applications. These topologies were created by either utilizing inherent rcr properties of differential mechanisms or combination between a differential and rcr mechanism from the two tables.

### 4.1 Topology matrices

The topology matrices are built as explained in section 2.2. Every mechanism found is given a name for later reference, both the mechanism found in literature or self made topologies. Self made topologies are depicted with a red border, they may exist in literature or industry but were not directly found during the search.

#### 4.1.1 Differential mechanisms

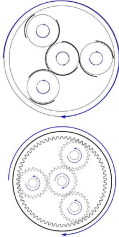
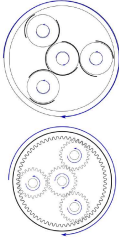
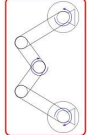
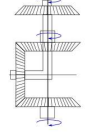
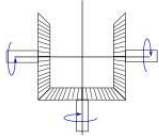
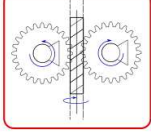
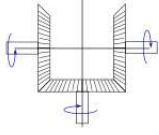
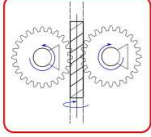
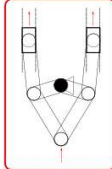
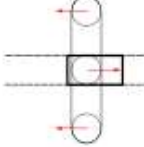
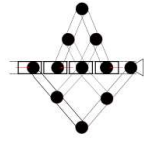
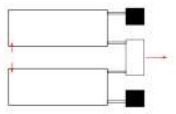
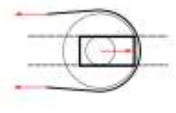
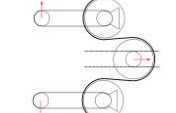
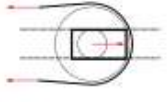
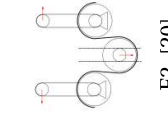
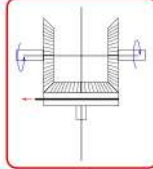
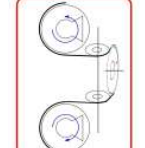
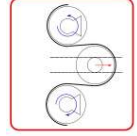
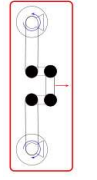
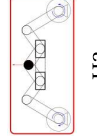
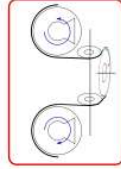
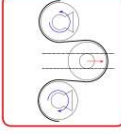
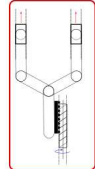
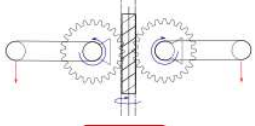
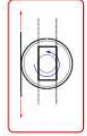
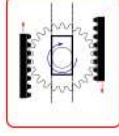
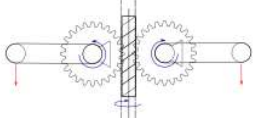
Table 3 shows the results found for differential mechanisms. The "inbetween output" column means that the output can be between parallel and perpendicular with respect to the input(s). The "Force to torque" row depicts mechanisms that have 1 force in- or output and 2 torque in-or outputs. the "Torque to force" row has it vice versa. The red arrows show in-/ output forces and the blue circular arrows in-/ output moments.

#### 4.1.2 Remote center of rotation mechanisms

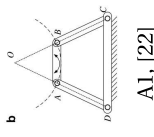
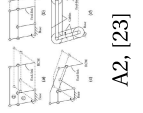
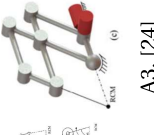
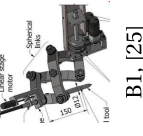
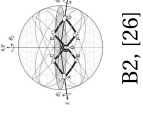
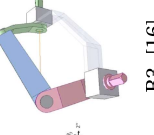
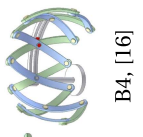
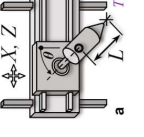
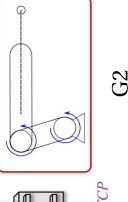
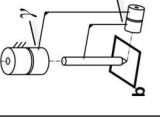
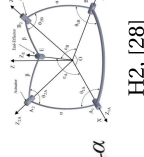
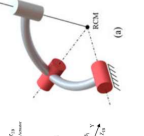
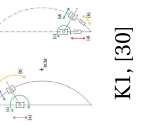
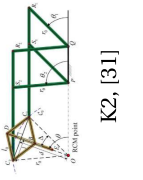
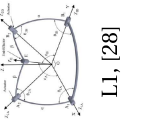
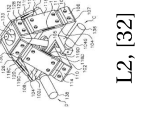
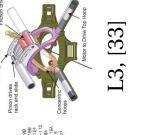
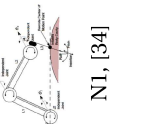
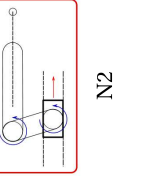
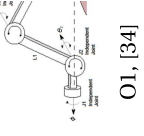
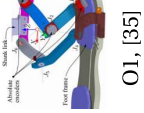
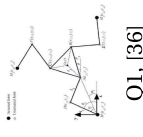
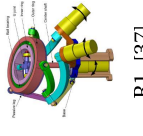
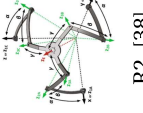
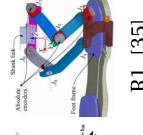
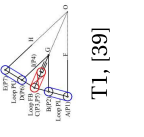
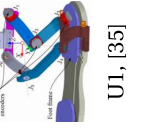
Table 4 shows the results found for rcr mechanisms. Serial and parallel inputs are used as differentiation on how the system can be "actuated". A certain mechanism can also be in both rows when multiple joints can be actuated. The "1 DoF" rows do not have a distinction between serial and parallel.

The "spatial" column is almost left empty as no real effort is gone into searches for the specific entries but is still kept in to keep the matrix complete. Important to note is that a mechanism can easily be changed from a 1 DoF system to 2 or 3 if that is necessary to accommodate to the freedom of the hip joint.

**Table 3:** The differential mechanism matrix. Red borders depict a self identified mechanism. The rows depict the transmission type and the columns the topology of the input and output w.r.t. each other.

	Parallel output				Perpendicular output		Inbetween output	
Torque to torque	 A1, [13]  A2, [14]  A3  A4, [13]	 B1, [15]  B2	 C1, [15]  C2					
Force to force	 D1  D2, [15, 13]  D3, [16]	 E1, [17, 18, 19]  E2, [15, 13]  E3, [20]	 F1, [15, 13]  F2, [20]					
Force to torque	 G1  G2	 H1  H2  H3	 I1  I2					
Torque to force	 J1  J2, [21]	 K1  K2	 L1, [21]					

**Table 4:** The Remote center of rotation matrix. Red borders depict a self identified mechanism. The rows depict the amount of actuators needed and the columns the spatial orientation.

	Planar		Spherical		Spatial
1 DoF Input	 A1, [22]  A2, [23]  A3, [24]	 B1, [25]  B2, [26]  B3, [16]  B4, [16]			
2 DoF Serial input	 G1, [27]  G2	 H1, [27]  H2, [28]  H3, [24]			 I1, [29]
2 DoF Parallel input	 K1, [30]	 K2, [31]	 L1, [28]  L2, [32]  L3, [33]		
3 Dof Serial input	 N1, [34]	 N2	 O1, [34]  OI, [35]		
3 Dof Parallel input	 Q1, [36]		 R1, [37]  R2, [38]  Rl, [35]		
3 Dof Serial/Parallel input	 T1, [39]		 U1, [35]		

## 4.2 Application designs

Mechanism B1/C1, G2/I1 and A4 from table 3 were identified as differential mechanisms with an inherent rcr. As the mechanism needs to span from the left to the right hip, a large distance needs to be covered. Thereby a pure scaling would not work for mechanism B1, so a slight variation was made, shown in figure 5. Figures 6 and 7 show 2 variations on mechanism G2, the pulley are connected by a guided rope. Figure 8 shows a possible topology for mechanism A4. For all mechanisms, the rotation axis are depicted and the inputs are shown with arrows and in black.

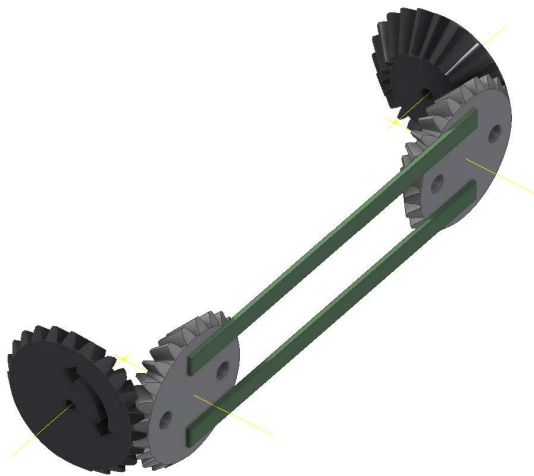


**Figure 5:** Differential mechanism with remote center of rotation based on B1.

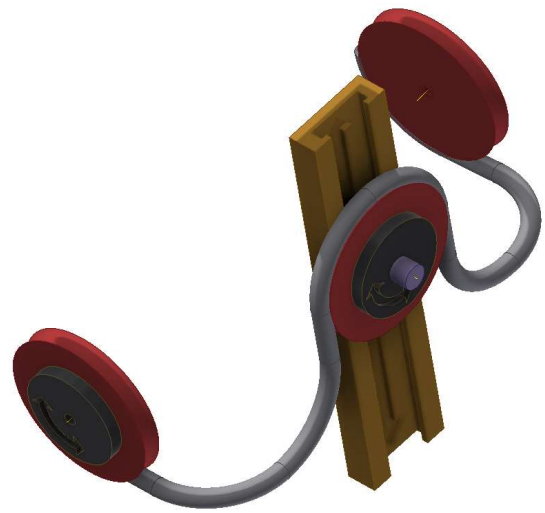


**Figure 6:** Differential mechanism with remote center of rotation based on G2, the grey rope is a guided cable.

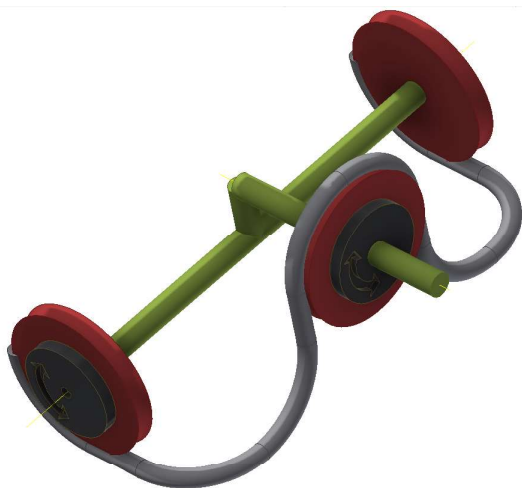


**Figure 7:** Differential mechanism with remote center of rotation based on G2, the grey rope is a guided cable.

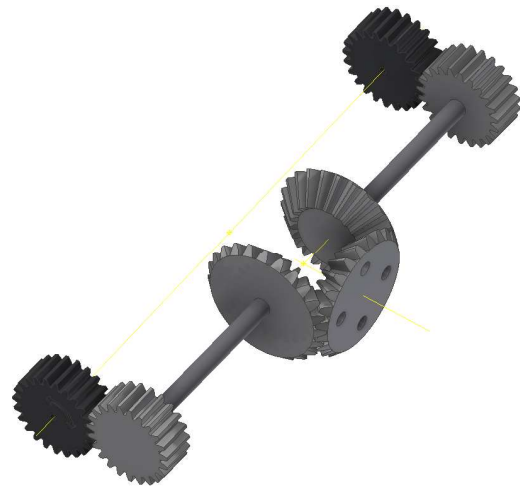


**Figure 8:** Differential mechanism with remote center of rotation based on A4.

Next, combinations are to be made between differential and rcr mechanism. Mechanisms A4,D2,H1 and H2 were found suitable for usage in an exoskeleton. The reasons being: Having an inherent size advantage, having

favorable in-/output directions or complexity.

Figure 8 shows a design based on mechanism A4, utilizing no rcr as none is needed for its direct function. Figure 9 is based on mechanism D2 combined with rcr mechanism B4. This rcr mechanism is chosen out of convenience and is not necessarily the best option. Figure 10 is based on mechanism H2 and utilizes rcr B3, again chosen due to convenience. Figure 11 makes use of the same rcr mechanism but combines it with differential mechanism H2.



**Figure 9:** Combination between differential mechanism D2 with remote center of rotation H3.



**Figure 10:** Combination between differential mechanism H1 with remote center of rotation B3.

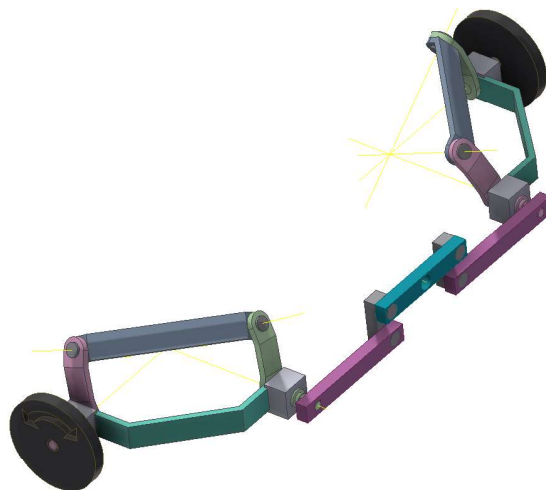


**Figure 11:** Combination between differential mechanism H2 with remote center of rotation B3.

## 5 Discussion

This section starts by discussing the whole report and in particular evaluate the results. Next, the possibilities of future research are examined. Highlighting the value this research can give.

### 5.1 Evaluation

The two topology matrices prove to be a good method to create feasible designs for exoskeleton applications. Although most mechanisms, both differential and rcr ones, are unused, no effort is lost as all can be useful nonetheless. The rcr mechanisms are underused more in this report but can prove a great asset once an actual design is to be made. A lot more combinations can be made out of the two topology matrices then are given in this report, which gives a lot of material for others to work with as well.

Some clear points can be taken away from the applications designs made, as it can firstly be seen that all designs utilize either gears, linkages or pulleys. Gears have a great range of motion, can easily be looped around corners and can be of relative low weight. It however needs good pre-tension and can be prone to wear. Linkages are lightweight, do not suffer from pre-tension. They however need a rcr mechanism and lack a great range of motion or become pretty bulky in the process. Pulley systems are inherently easier to loop around angles, can be lightweight and have a good range of motion. The wear and tear do cause problems on the long term and are hard to get rid of.

### 5.2 Future research

A compliant version of the proposed designs could be a feasible solution for actual application in an exoskeleton, as such a mechanism will get rid of most wear and pre-tension. Also the use of shell-mechanisms should not be excluded. No such mechanism was however found, meaning a lot of opportunity. It will however be a challenge to limit the stiffness of the mechanism ones compliant elements are added, as compliant joints will likely have inherent stiffness. Compliant mechanisms mostly suffer from a low range of motion but this should not necessarily be an issue, as no continuous revolutions need to be made within an exoskeleton application.

It is advised to dive into literature again for any future research, but instead look into compliant or shell subsystems to tackle the shortcomings of these classical mechanisms while keeping the topology mostly intact.

## 6 Conclusion

A literature study is done to characterize both differential and remote center of rotation (rcr) mechanisms, to utilize in exoskeleton applications. The ACCREx method is used to create complete topology matrices, which prove to be a good tactic to systematically create solutions. Suitable mechanical topologies are generated by exploiting the inherent rcr properties of a differential mechanism or by combining mechanisms from both matrices.

The combination topologies all have their ups and downs but are not a final solution. To make or find a final topology for an exoskeleton application, it is advised to change subsystems to include more compliant parts and counteract shortcomings like pre-tension and wear and tear. So to conclude, this report gives a complete view on classical differential and remote center of rotation mechanisms, but it does not facilitate a completely feasible topology. For that, compliant or shell mechanisms need to be investigated.

## References

- [1] Allied Analytics LLP. Smart Exoskeleton Market by Component, Type, Body Part and Application: Global Opportunity Analysis and Industry Forecast, 2018 - 2025, 2019.
- [2] Nick Augustejn. Ford medewerkers krijgen exoskelet, retrieved from <https://www.autoweek.nl/autonieuws/artikel/ford-medewerkers-krijgen-exoskelet/>, 2018.
- [3] Sean Szymkowski. Hyundai shows off exoskeleton robot to help assembly line workers, retrieved from <https://www.cnet.com/roadshow/news/hyundai-exoskeleton-vest-robot/>, 2019.
- [4] Tim Bosch, Jennifer van Eck, Karlijn Knitel, and Michiel de Looze. The effects of a passive exoskeleton on muscle activity, discomfort and endurance time in forward bending work. *Applied Ergonomics*, 54:212–217, 2016.
- [5] S. J. Baltrusch, J. H. van Dieën, S. M. Bruijn, A. S. Koopman, C. A.M. van Bennekom, and H. Houdijk. The effect of a passive trunk exoskeleton on metabolic costs during lifting and walking. *Ergonomics*, 62(7):903–916, 2019.
- [6] Laevo. Laevo, retrieved from <http://en.laevo.nl/> at 14-01-2020.
- [7] SuitX. SuitX, retrieved from <https://www.suitx.com/> at 14-01-2020.
- [8] IFtoMM. Terminology for the theory of machines and mechanisms. *Mech. Mach. Theory*, 26(5):435–539, 1991.
- [9] Matthias B. Naf, Karen Junius, Marco Rossini, Carlos Rodriguez-Guerrero, Bram Vanderborght, and Dirk Lefebber. Misalignment Compensation for Full Human-Exoskeleton Kinematic Compatibility: State of the Art and Evaluation. *Applied Mechanics Reviews*, 70(5), 2018.
- [10] Karen Junius, Marc Degelaen, Nina Lefebber, Eva Swinnen, Bram Vanderborght, and Dirk Lefebber. Bilateral, Misalignment-Compensating, Full-DOF Hip Exoskeleton: Design and Kinematic Validation. 2017, 2017.
- [11] Paul Breedveld, Just L. Herder, and Tetsuo Tomiyama. Teaching creativity in mechanical design. *Diversity and unity: Proceedings of IASDR*, 2011.
- [12] Massimo Cenciarini and Aaron M. Dollar. Biomechanical considerations in the design of lower limb exoskeletons. *IEEE International Conference on Rehabilitation Robotics*, pages 10–14, 2011.
- [13] Nicholas P Chironis. *Mechanisms and mechanical devices sourcebook*, volume 49. 2012.
- [14] Jesse R Cannon, Craig P Lusk, and Larry L Howell. compliant rolling-contact element mechanisms. Technical report, 2005.
- [15] Lionel Birglen and Clément M. Gosselin. Force analysis of connected differential mechanisms: Application to grasping. *International Journal of Robotics Research*, 25(10):1033–1046, 2006.
- [16] Nguyen Duc Thang. 1700 animated mechanical mechanisms. 2014.
- [17] Ditske J. B. A. de Lange, Matthijs Langelaar, and Just L. Herder. Towards the Design of a Statically Balanced Compliant Laparoscopic Grasper using topology optimization. (December 2015), 2008.

- [18] Ronald A J Stavenuiter, Lionel Birglen, and Just L Herder. A planar underactuated grasper with adjustable compliance. *Mechanism and Machine Theory*, 112:295–306, 2017.
- [19] Lionel Birglen and Clément M. Gosselin. Force analysis of connected differential mechanisms: Application to grasping. *International Journal of Robotics Research*, 25(10):1033–1046, 2006.
- [20] Raymond R. Ma, Lael U. Odhner, and Aaron M. Dollar. A modular, open-source 3D printed underactuated hand. *Proceedings - IEEE International Conference on Robotics and Automation*, pages 2737–2743, 2013.
- [21] Kuat Telegenov, Yedige Tlegenov, and Almas Shintemirov. An underactuated adaptive 3D printed robotic gripper. *10th France-Japan Congress, 8th Europe-Asia Congress on Mechatronics, MECATRONICS 2014*, pages 110–115, 2014.
- [22] Guanghua Zong, Xu Pei, Jingjun Yu, and Shusheng Bi. Classification and type synthesis of 1-DOF remote center of motion mechanisms. *Mechanism and Machine Theory*, 43(12):1585–1595, 2008.
- [23] Jianmin Li, Guokai Zhang, Yuan Xing, Hongbin Liu, and Shuxin Wang. A class of 2-degree-of-freedom planar remote center-of-motion mechanisms based on virtual parallelograms. *Journal of Mechanisms and Robotics*, 6(3):1–7, 2014.
- [24] Uikyum Kim, Dong Hyuk Lee, Yong Bum Kim, Dong Yeop Seok, Jinho So, and Hyouk Ryeol Choi. S-Surge: Novel Portable Surgical Robot with Multiaxis Force-Sensing Capability for Minimally Invasive Surgery. *IEEE/ASME Transactions on Mechatronics*, 22(4):1717–1727, 2017.
- [25] Julius Lipskas, Kamal Deep, and Wei Yao. Robotic-Assisted 3D Bio-printing for Repairing Bone and Cartilage Defects through a Minimally Invasive Approach. *Scientific Reports*, 9(1):1–9, 2019.
- [26] Miguel Nobre Castro, John Rasmussen, Michael Skipper Andersen, and Shaoping Bai. A compact 3-DOF shoulder mechanism constructed with scissors linkages for exoskeleton applications. *Mechanism and Machine Theory*, 132:264–278, 2019.
- [27] Carsten Teichgräber, Jörg Müglitz, and Maik Berger. Guiding linkages with remote centre of rotation for thermal cutting processes. *Mechanisms and Machine Science*, 52:21–30, 2018.
- [28] Terence Essomba and Linh Nguyen Vu. Kinematic analysis of a new five-bar spherical decoupled mechanism with two-degrees of freedom remote center of motion. *Mechanism and Machine Theory*, 119:184–197, 2018.
- [29] Prasanna S. Gandhi, Rupesh S. Bobade, and Chao Chen. On novel compliant mechanisms for remote center motion. *Advances in Mechanical Engineering*, 10(4):1–11, 2018.
- [30] Hiu Man Yip, Peng Li, David Navarro-Alarcon, Zerui Wang, and Yun Hui Liu. A new circular-guided remote center of motion mechanism for assistive surgical robots. *2014 IEEE International Conference on Robotics and Biomimetics, IEEE ROBIO 2014*, pages 217–222, 2014.
- [31] Genliang Chen, Jiepeng Wang, and Hao Wang. A new type of planar two degree-of-freedom remote center-of-motion mechanism inspired by the peaucellier-lipkin straight-line linkage. *Journal of Mechanical Design, Transactions of the ASME*, 141(1), 2019.

- [32] Yves Bellouard. Remote center of rotation positioning device, 2007.
- [33] Conor J Walsh, Nevan C Hanumara, Alexander H Slocum, and Jo-anne Shepard. A Patient-Mounted, Telerobotic Tool for CT-Guided Percutaneous Interventions. *Journal of Medical Devices*, 2(March), 2008.
- [34] Suraj Parameswaran, Karthik Chandrasekaran, Sourav Chandra, and Asokan Thondiyath. Optimisation of an active remote centre of motion mechanism for minimal extracorporeal workspace for robotic surgery. *ACM International Conference Proceeding Series*, pages 0–5, 2013.
- [35] Man Bok Hong, Gwang Tae Kim, and Yeo Hun Yoon. ACE-Ankle: A Novel Sensorized RCM (Remote-Center-of-Motion) Ankle Mechanism for Military Purpose Exoskeleton. *Robotica*, 2019.
- [36] A. Noshadi and M. Mailah. Fuzzy-based active force with computed torque control of 3-RRR parallel robotic manipulator. *International Review on Modelling and Simulations*, 4(5):2666–2676, 2011.
- [37] Guanglei Wu, Stéphane Caro, and Jiawei Wang. Design and transmission analysis of an asymmetrical spherical parallel manipulator. *Mechanism and Machine Theory*, 94:119–131, 2015.
- [38] Terence Essomba, M. A. Laribi, Y Hsu, and S Zeghloul. Kinematic analysis of a 3-RRR spherical parallel mechanism with configurable base. In *Mechanisms and Machine Science*, volume 66, pages 101–109. 2019.
- [39] S. Liu, B. Chen, S. Caro, S. Briot, L. Harewood, and C. Chen. A cable linkage with remote centre of motion. *Mechanism and Machine Theory*, 105:583–605, 2016.



# B

## Warping theory

Torsion applied to a beam will cause it to deform. For structures with a circular cross section, this deformation will be purely in plane with respect to its cross section [6, 16]. For non axisymmetric cross sections a secondary deformation occurs, warping. Warping is defined by Vlasov [18] as: "the distortion of the plane section caused by longitudinal displacements".

The applied torsion can thereby be classified as uniform or non-uniform torsion. Uniform torsion is also called St. Venant torsion after his original theorem [14]. Uniform torsion will result in a constant twist angle over the length of the beam, implying  $\theta' = 0$ . An illustration of uniform torsion is shown in Figure B.1. The torsion constant  $J$  is defined as the resistance of a beam against pure or uniform torsion [5]. Non-uniform torsion has a non-constant deformation angle over its length, or  $\theta' \neq 0$  in other words. Figure B.2 shows this non-uniform torsion due to a symmetric load with a constraint on the centre plane.



Figure B.1: Uniform torsion of a beam under torsional load.

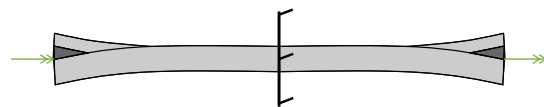


Figure B.2: Non-Uniform torsion of a beam under torsional load.

The resulting twist of the beam due to the applied torque is around the so called "shear center" [5]. This geometric property is defined as "the point in the plane of the cross section about which twisting takes place" [5]. Which is different from the centroid of a beam, defined as center of mass of a cross section. For an I-beam, the shear center is located at the center web, but for a channel-beam it is located outside of the material. Figure B.3 illustrates the location of the centroid and shear center for different cross sections.

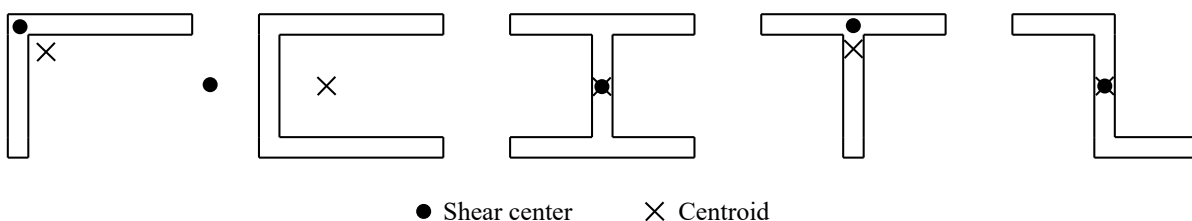


Figure B.3: The location of the centroid and shear center for various cross sections.

For the following given theories regarding warping, assumptions are made. The material is assumed to be homogeneous, isotropic and linearly elastic [6, 13]. The wall thickness is also presumed to be thin-walled [6], which according to Vlasov is defined as  $\delta/d \leq 0.1$ . With  $\delta$  being the thickness and  $d$  the cross section characteristic dimension [18].

## B.1. Warping displacement

The warping displacement  $w$  is defined as the out of plane displacement of a CS as a function of location on the cross section. A rotation per unit length  $\theta$  is applied, with Figure B.4 showing an arbitrary cross section. Due to the applied rotation, every point on this cross section becomes inclined with respect to point O by  $\rho\theta$ . Due to torsion a relative angle  $\alpha$  exists between the tangent and the z-y plane of  $\rho\theta\cos(\alpha) = r\theta$  [16].

With the perpendicular distance  $r$  and distance  $s$  from the defined origin of the section, the relation of Equation B.1 is obtained [16]. Equation B.2 is obtained by integrating, with  $w_0$  denoting "the displacement in the x-direction of the point from which  $s$  is measured" [16].

$$\frac{\partial w}{\partial s} = -r\theta \quad (\text{B.1})$$

$$w = w_0 - \theta \int_0^s r ds \quad (\text{B.2})$$

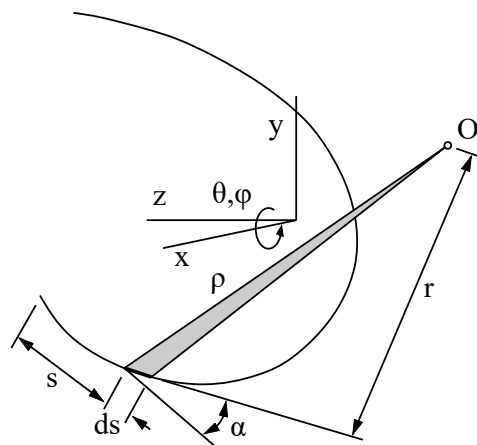


Figure B.4: Parameters used to determine the warping displacement. Illustration adapted from Timoshenko [16].

If the point O is now assumed to be the shear center, the equation can be solved. Equation B.3 gives the equation for the warping of a point on the cross section with respect to point O [13, 16].

$$\begin{aligned} w &= \theta (\bar{\omega}_s - \omega_s) \\ \omega_s &= \int_0^s r ds \\ \bar{\omega}_s &= \frac{1}{A} \int_0^A \omega_s ds \end{aligned} \quad (\text{B.3})$$

With  $\omega_s$  being called the "warping function", represents the doubled sectorial area corresponding to the arc  $s$  of the middle line of the cross section, while  $\bar{\omega}_s$  is the average value of  $\omega_s$  [16] and  $A$  is the area of the cross section. The average is used to compensate for the distance between the shear center and the point from which  $s$  is measured, as the average is zero when it is measured from the shear center itself.

## B.2. Torsion formula

A non cylindrical beam can resist torsion in two ways, by St. Venant and warping torsion [11]. In Figure B.5(a), torsion is applied to the web of an I-beam, resulting in the internal moments as shown in Figure B.5(b).

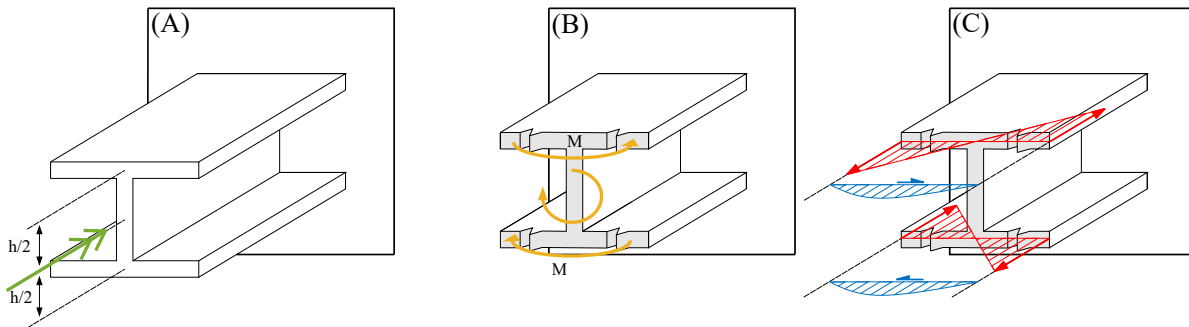


Figure B.5: (a) shows the applied torsion, (b) the resulting moments in the section and (c) the corresponding stresses.

Equation B.4 shows the sum of the pure torsional moment  $T_p$  and the warping torsional moment  $T_w$  [6, 7, 11, 18], with  $T_{tot}$  being the total torsional moment at a cross section.  $\phi'$  is the derivative of angle of rotation with respect to the distance along the length. The factor  $B$  is called the bimoment and is defined by Equation B.5, with  $M$  the bending moment in the flanges and  $h$  the distance between the flanges of the I-beam.

$$\begin{aligned} T_{tot} &= T_p + T_w \\ &= GJ\phi' - EI_w\phi''' \end{aligned} \quad (B.4)$$

$$\begin{aligned} B &= Mh \\ &= -EI_w \cdot \phi'' \end{aligned} \quad (B.5)$$

$$\phi = Tl/GJ \quad (B.6)$$

The bimoment is an immeasurable quantity but is used to talk about the 7<sup>th</sup> DoF of a beam. The 7<sup>th</sup> DoF is used to describe restrained warping, as it "allows" for out of plane movement of the cross section. This 7<sup>th</sup> DoF relates to the derivative of the rotation in the displacement vector. This bimoment is also independent of the shear centre and of the origin of the sectorial area [18].

## B.3. Torsion stresses

The resulting stresses due to the applied torque can be seen in Figure B.5. Uniform torsion only results in shear stresses, whereas warping torsion results in both normal and shear stresses [11]. Equation B.7 is used to calculate the peak St. Venant shear stress, utilizing the relation given in Equation B.6. With the stress being maximum on the surface and only being valid for constant thickness sections [7].

$$\begin{aligned} \tau &= Gt\phi' \\ &= Tt/J \end{aligned} \quad (B.7)$$

If warping torsion is considered, different formulæ must be applied. The peak normal stresses resulting from warping of the cross section are given by Equation B.8, with the maximum at the flange tip [7, 9].  $W_n$  is called the "normalized warping function" [7].

With  $S_w$  being called the "warping statical moment" [7]. Both  $S_w$  and  $W_n$  being standard values for certain cross sections, as well as being location dependent [7]. The values change between the web junction and the tip of the flange. A visualization of the distribution of the stress is given in Figure B.5.

$$\sigma_w = \pm EW_n \phi'' \quad (\text{B.8})$$

$$\tau_w = ES_{w1} \phi''' / t \quad (\text{B.9})$$

## B.4. Warping stiffness

Equation B.5 refers to  $I_w$ , which is called the warping constant. This geometric property measures the resistance of a structural member to nonuniform or warping torsion [5]. It can be interpreted as the resistance against warping deformation or torsion.  $I_w$  has units of length to the sixth power [13, 16], and is also called the second moment of inertia [18]. The warping constant is defined as followed [6, 13, 16, 18]:

$$\begin{aligned} I_w &= \int_0^m (\bar{\omega}_s - \omega_s)^2 t ds \\ \omega_s &= \int_0^s r ds \\ \bar{\omega}_s &= \frac{1}{A} \int_0^A \omega_s ds \end{aligned} \quad (\text{B.10})$$

For T-, V- or L-profiles, the perpendicular distance  $r$  (Figure B.4) reduces to zero, thereby having a warping constant of zero [13, 16]. Figure B.6 shows the kinds of structures with a very low warping constant, for which secondary warping can occur. These secondary stresses occur if the thickness is not too thin or vary over the thickness of the cross section [13]. If these kinds of structures are utilized, a secondary warping constant should be taken into account.

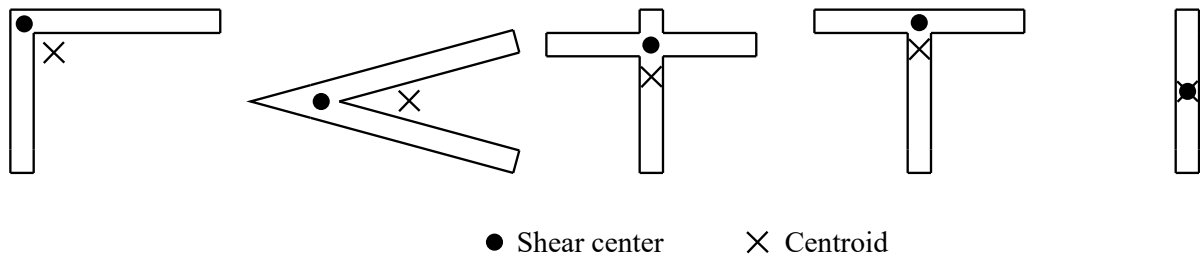


Figure B.6: Examples of shapes with a zero warping constant.

The torsion rigidity or stiffness is defined as  $GJ$  [13], with  $G$  being the shear modulus and  $J$  the torsional constant [11]. The torsional constant can also be referred to as the St. Venant torsional constant [7].  $EI_w$  is called the warping rigidity, with  $E$  being the elastic modulus and  $I_w$  the previously mentioned warping constant.

## B.5. Twist

Equation B.5 shows the solved differential equation for determining the rotation angle along the length of the beam  $x$  [7], with  $\phi_p$  the particular solution [13].  $c$  is called the torsional bending constant, describing the decline of the warping torsional moment from the constrained to free state along the length of a beam [6, 7, 13, 18].

$$\begin{aligned} \phi &= A_0 + A_1 x + A_2 e^{cx} + A_3 e^{-cx} + \phi_p \\ c &= GJ/EI_w \end{aligned} \quad (\text{B.11})$$

To obtain a specific solution, boundary conditions are needed. The three most used end conditions are given, a fixed-end condition implies no rotation and no warping, a simply supported end implies a fork support and the free-end support cannot twist and is free of normal stress [7, 13].

- Fixed-end:  $\phi = 0, \quad d\phi/dx = 0$
- Simply supported end:  $\phi = 0, \quad d^2\phi/dx^2 = 0$
- Free-end:  $d^2\phi/dx^2 = 0, \quad d^3\phi/dx^3 - c^2d\phi/dx = 0$

An example is worked out for a beam being fixed at one side, with the input being free as shown in Figure B.5 [13]. For the analysed example, Equation B.5 reduces to:

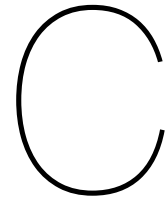
$$\phi = A_0 + A_2 e^{cx} + A_3 e^{-cx} + \phi_p$$

$$\phi = \frac{d\phi}{dx} = 0 \quad \text{at } x = 0 \quad \text{and} \quad \frac{d^2\phi}{dx^2} = 0 \quad \text{at } x = L$$

is solved to be

$$\phi = \frac{T}{cGJ} [\tanh cL(\cosh cx - 1) - \sinh cx + cx]$$





## Test setup

This chapter presents the experimental setup used to obtain the data. Photos are used to show the different components, how the tests are run and how the data is collected. A difference is made between the two load cases, both shown in separate section.

### **C.1. Load case 1**

Figure C.1 and C.2 show the total overview of the setup used for load case 1 from different angles. Figure C.3 shows the input side of the experimental setup, including the inclinometer, misalignment coupling and constraint. Figure C.4 shows the output inclinometer with output constraint and ball support. Figure C.5 and C.6 show the input and center constraint.

The aluminium (black) profile, shown in Figure C.6, is used to "zero" the input and output inclinometer with respect to the bottom plate. An experiment is done by first connecting the sensors to the LabVIEW script. Next a cycle of 5 positive and negative input rotations is performed to gain the data for 1 test for 1 orientation. This is done for 2 orientations twice, resulting in a total of 4 datasets. The deformed states of beam Z and C are shown in Figure C.7 and C.8 respectively.

### **C.2. Load case 2**

An overview of the experimental setup for load case 2 can be seen in both Figure C.9 and C.10. Figure C.11 shows the center constraint used to test for load case 2, a fixed constraint is applied to the center cross section as only half of the beam is used. Figure C.12 shows the input side of the experiment setup.

The same zero method is used for load case 2 as for load case 1. With the data again obtain via LabVIEW. The experiments are done by pushing and pulling the bolt connected to the load cell, for a total of 10 times per test. For two orientation the tests are done twice, resulting in 4 datasets in total. Figure C.13 and C.14 show an relaxed and deformed state of the system.

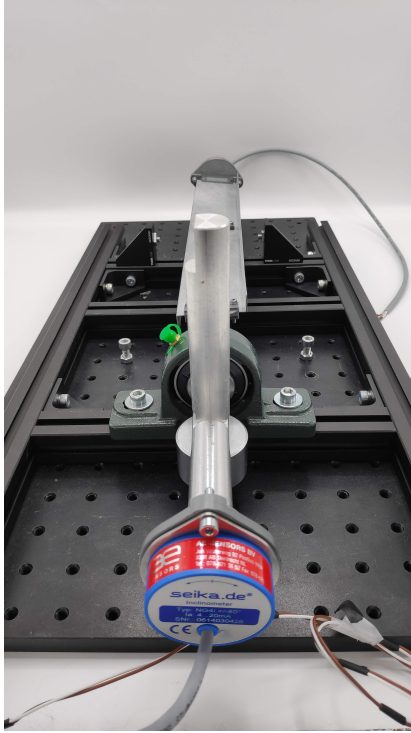


Figure C.1: Total overview of the experimental setup shown for load case 1 from the front.

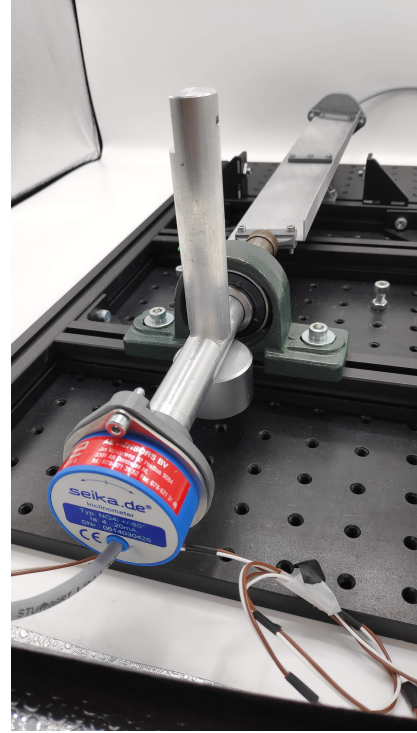


Figure C.2: Total overview of the experimental setup shown for load case 1 from the side.

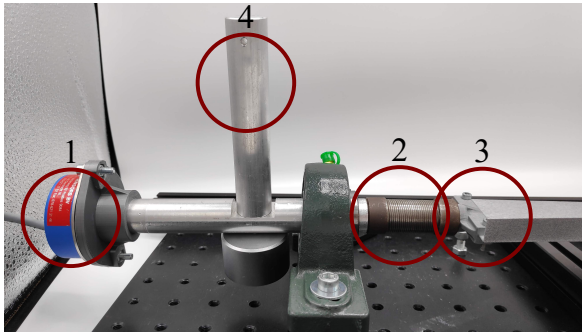


Figure C.3: Side view of the input side of the experiment for load case 1. (1) is the input inclinometer, (2) the misalignment coupling, (3) the connection piece to the analysed beam and (4) the lever used to apply a rotation.

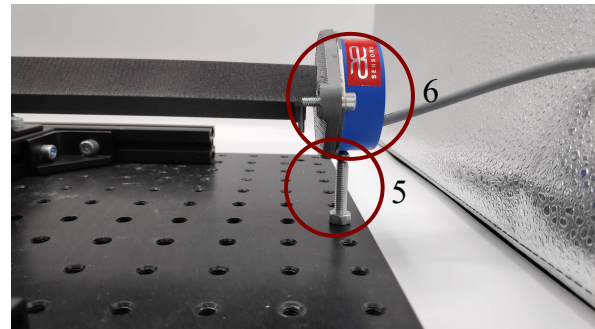


Figure C.4: Side view of the output side of the experiment for load case 1. (5) is the ball contact to compensate for the weight of the inclinometer and (6) the output inclinometer.

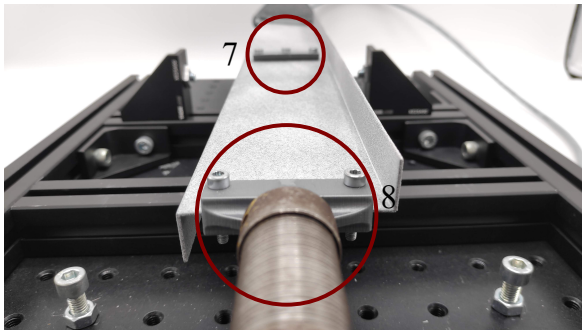


Figure C.5: Front view of the constraints of the experiments for load case 1. (7) is the center constraint and (8) shows the input misalignment coupling and input constraint.

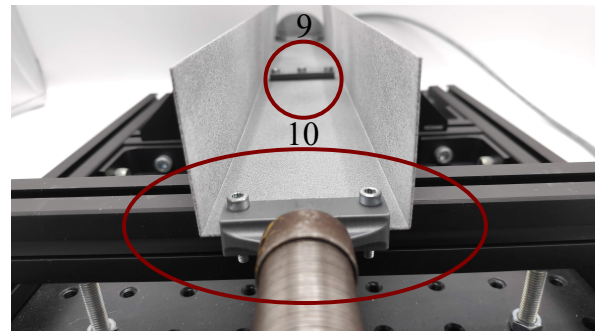


Figure C.6: Front view of the constraints of the experiments for load case 1. (9) is the center constraint and (10) show the input misalignment coupling and input constraint. The profile under the beam is used to level the inclinometer with respect to the bottom plate.

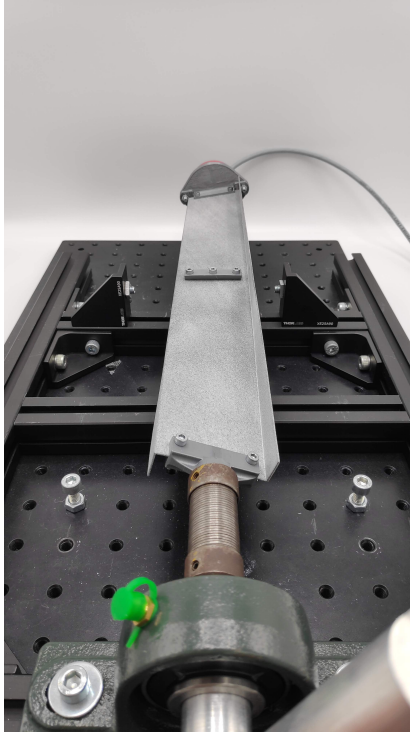


Figure C.7: Front view of the deformed Z beam for load case 1.

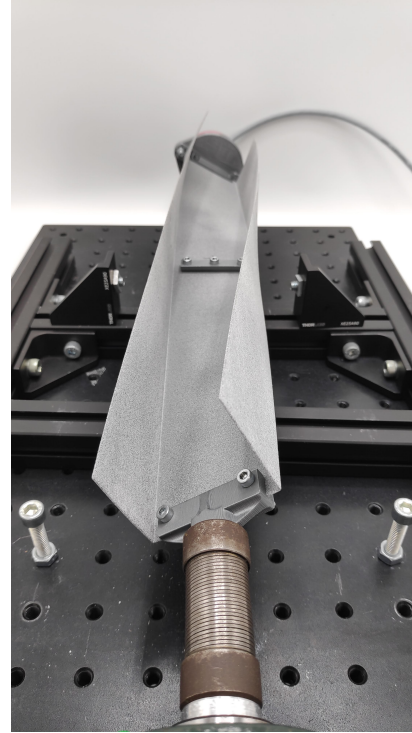


Figure C.8: Front view of the deformed C beam for load case 1.



Figure C.9: Total overview of the experimental setup shown for load case 2 from the front.

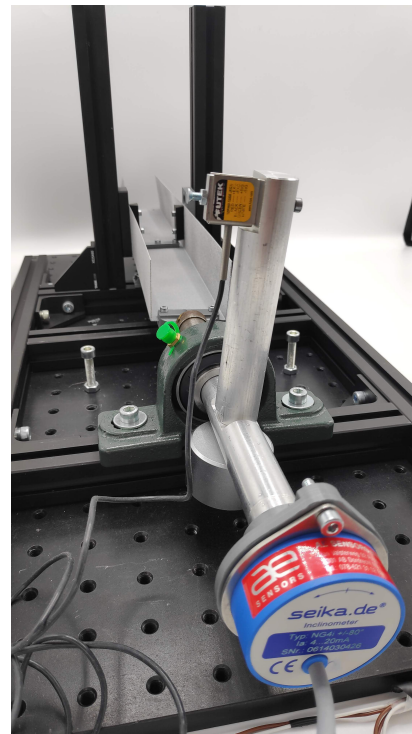


Figure C.10: Total overview of the experimental setup shown for load case 2 from the side.

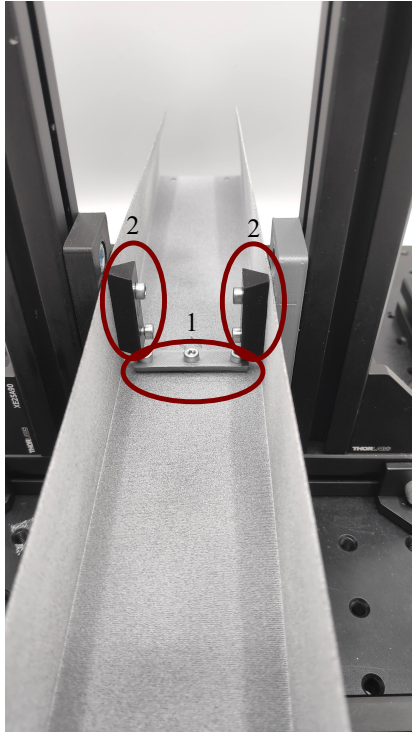


Figure C.11: Front view of the center constraint for load case 2. (1) shows the same constraint used in load cases 1, with (2) showing the two extra constraint used for the flanges to create a fixed center cross section.

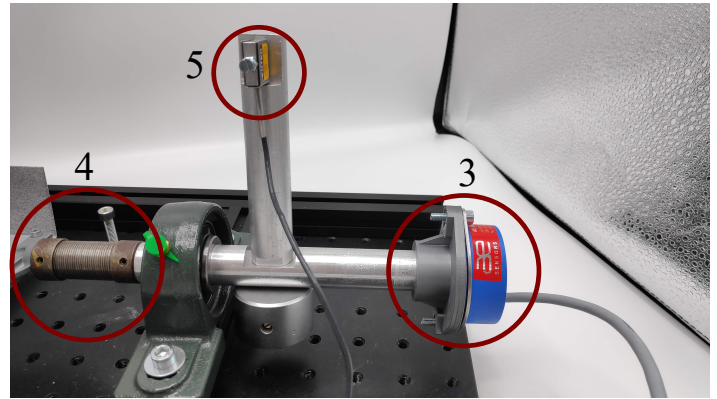


Figure C.12: Side view of the input for load case 2. (3) is the inclinometer measuring the twist under the applied torque. (4) shows the coupling to the beam, with (5) showing the load cell to measure to input torque.

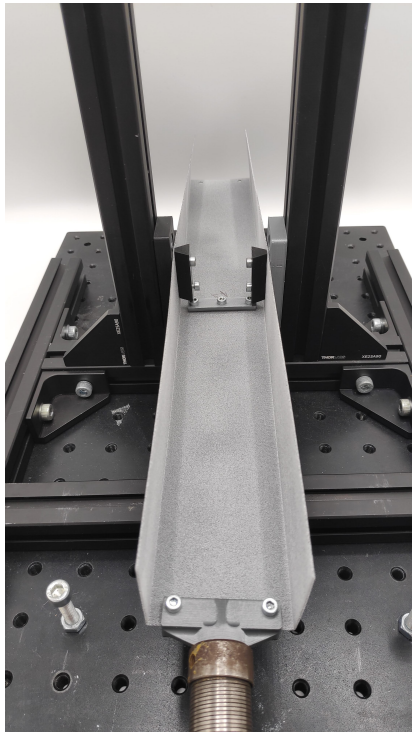


Figure C.13: Front view of the undeformed C beam for load case 2.

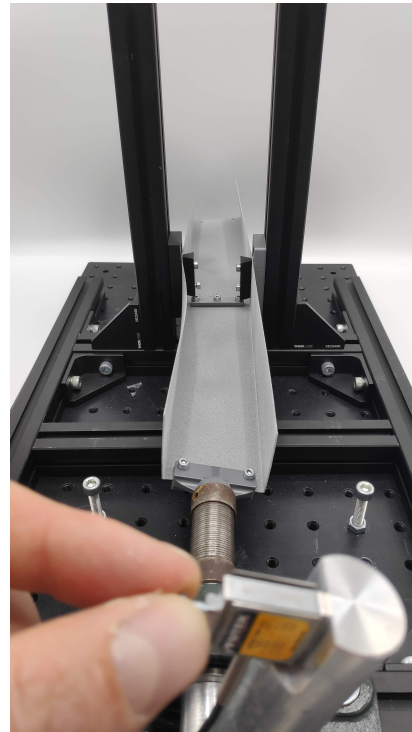
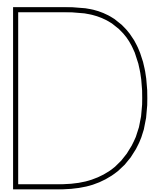


Figure C.14: Front view of the deformed C beam for load case 2.



## Matlab and Ansys code

This chapter shows the code used to run ANSYS APDL from MATLAB. First, the cross section parameters are computed in MATLAB and the load case and cross section type are specified. Next, the ANSYS model is opened and run with the given inputs. The ANSYS model saves its data for MATLAB to load in again, completing the cycle.

The provided code is for the shell model. If another model is preferred, only the ANSYS code has to be changed as no model is selected in MATLAB.

```

% combination script for pre and post processing of ansys model
% Maurice Valentijn
clc
clear all
close all
addpath('D:\tudelft 2019-2020\Thesis project -\software\Ansys\
    Cross_sections')
Params1

%% Determining cross-section --> copied to ansys --> copy to startup ansys
part
crossection= 'Z'; % 'T' 'Rectangle' 'Circle' 'Circular_tube' 'I' '
    Rect_tube' 'Chan' 'Z' 'L' 'Half_circle' 'Elips' 'Hat' 'IHat'
Loading= 'Torque'; % 'Rotation' 'Torque'
% Loading= 'Torque'; % 'Rotation' 'Torque'
% !!!!!!!!!!!!! Also change these parameters in the output part
%amount_of_cs=6;
amount_of_kp=1;
max_amount_param=4; % number of output parameters from ansys

%% Pre processing --> calling upon the "optimization" scrips for different
cases

if strcmp (crossection, 'Chan')
    % needed for cross section: W1,W2="length of flanges",W3="overall
    depth",
    % t1,t2="flange thicknesses", t3="web thickness"
    [b,h,t,bc,hc,tc, Optimize_cases_v2, J_within_range_cJ, C_within_range_cJ,
    J_within_range_cC, C_within_range_cC]=...
    Pre_warping_beam_Chan_profile_v2(steps,A_max,b_min,h_min,t_min,b_max,h_max,
    t_max,search_percentage_J,search_percentage_C,target_value_J,
    target_value_C);
    Optimize_cases=Optimize_cases_v2;
    amount_of_cs=length(t);
    %W1=1; W2=2; W3=3; T1=1; T2=2; T3=1;

elseif strcmp (crossection, 'Z')
    % needed for cross section: W1,W2="length of flanges",W3="overall
    depth",
    % t1,t2="flange thicknesses", t3="stem thickness"
    [b,h,t,bc,hc,tc, Optimize_cases_v2, J_within_range_cJ, C_within_range_cJ,
    J_within_range_cC, C_within_range_cC]=...
    Pre_warping_beam_Z_profile_v2(steps,A_max,b_min,h_min,t_min,b_max,h_max,
    t_max,search_percentage_J,search_percentage_C,target_value_J,
    target_value_C);
    Optimize_cases=Optimize_cases_v2;
    amount_of_cs=length(t);
    %W1=1; W2=2; W3=3; T1=1; T2=2; T3=1;

elseif strcmp (crossection, 'L')
    % needed for cross section: W1,W2="leg lengths"
    % t1,t2="leg thicknesses"
    [b,h,t,bc,hc,tc, Optimize_cases_v2, J_within_range_cJ, C_within_range_cJ,
    J_within_range_cC, C_within_range_cC]=...
    Pre_warping_beam_L_profile_v2(steps,A_max,b_min,h_min,t_min,b_max,h_max,
    t_max,search_percentage_J,search_percentage_C,target_value_J,

```

```

target_value_C);
    Optimize_cases=Optimize_cases_v2;
    amount_of_cs=length(t);
    %W1=1; W3=3; T1=1; T3=1;

    elseif strcmp (crossection, 'T')
        % needed for cross section: W1,W2="leg lengths"
    [b, h, t, bc, hc, tc, Optimize_cases_v2, J_within_range_cJ, C_within_range_cJ,
    J_within_range_cC, C_within_range_cC]=...
    Pre_warping_beam_T_profile_v2(steps, A_max, b_min, h_min, t_min, b_max, h_max,
    t_max, search_percentage_J, search_percentage_C, target_value_J,
    target_value_C);
    Optimize_cases=Optimize_cases_v2;
    amount_of_cs=length(t);
    %W1=1; W3=3; T1=1; T3=1;

    elseif strcmp (crossection, 'Half_circle')
        % needed for cross section: Radius, angle_inner, Radius_inner, angle
        /2
    [r, t, alfa, rc, tc, alfac, Optimize_cases_v2, J_within_range_cJ,
    C_within_range_cJ, J_within_range_cC, C_within_range_cC]=...
    Pre_warping_beam_Half_circle_profile_v2(steps, A_max, r_min, t_min, alfa_min,
    r_max, t_max, alfa_max, search_percentage_J, search_percentage_C,
    target_value_J, target_value_C);
    Optimize_cases=Optimize_cases_v2;
    amount_of_cs=length(t);
    %Radius=1; angle_inner=1; Radius_inner=1; angle=1;

    elseif strcmp (crossection, 'I')
        % needed for cross section: W1,W2="length of flanges", W3="overall
        depth",
        % t1, t2="flange thicknesses", t3="web thickness"
    [b, h, t, bc, hc, tc, Optimize_cases_v2, J_within_range_cJ, C_within_range_cJ,
    J_within_range_cC, C_within_range_cC]=...
    Pre_warping_beam_I_profile_v2(steps, A_max, b_min, h_min, t_min, b_max, h_max,
    t_max, search_percentage_J, search_percentage_C, target_value_J,
    target_value_C);
    Optimize_cases=Optimize_cases_v2 ;
    amount_of_cs=length(t);
    %W1=1; W2=2; W3=3; T1=1; T2=2; T3=1;

    elseif strcmp (crossection, 'Hat')
    [b, h, t, hh, bc, hc, tc, hhc, Optimize_cases_v2, J_within_range_cJ,
    C_within_range_cJ, J_within_range_cC, C_within_range_cC]=...
    Pre_warping_beam_Hat_profile_v2(steps, A_max, b_min, h_min, t_min, b_max, h_max,
    t_max, search_percentage_J, search_percentage_C, target_value_J,
    target_value_C)
    Optimize_cases=Optimize_cases_v2;
    amount_of_cs=length(t);
    %W1=1; W2=2; W3=3; W4=1 T1=1; T2=2; T3=1; T4=1; T5=1;

    elseif strcmp (crossection, 'IHat')
    [b, h, t, hh, bc, hc, tc, hhc, Optimize_cases_v2, J_within_range_cJ,
    C_within_range_cJ, J_within_range_cC, C_within_range_cC]=...
    Pre_warping_beam_IHat_profile_v2(steps, A_max, b_min, h_min, t_min, b_max, h_max,
    t_max, search_percentage_J, search_percentage_C, target_value_J,

```

```

target_value_C)
    Optimize_cases=Optimize_cases_v2;
    amount_of_cs=length(t);

end

%% Start loop to send and get results from ansys
Results_ansys=zeros(amount_of_kp,max_amount_param,amount_of_cs);
for i=1: amount_of_cs

%% BEGIN Txt export to ansys_input_crossection --> section properties
    needed for ansys
% crossection= 'Rectangle' 'Circle' 'Circular_tube' 'I_profile' '
    Rect_tube' 'Chan' 'Z' 'L' 'Half_circle' 'Elips' 'Hats'
% Loading= 'Rotation' 'Torque'

fid=fopen('D:\tudelft 2019-2020\Thesis project -\software\Ansys\
    Warping_shell_maurice_v3\Ansys_input_crossection.txt','wt');
fprintf(fid, 'crossection=' 'Z' ' \n' );
fprintf(fid, 'Loading=' 'Torque' ' \n' );
% fprintf(fid, 'Loading=' 'Torque' ' \n' );
%fprintf(fid, 'W1= %d \n', W1 );

%% loops

if strcmp (crossection, 'Rectangle')
    %Optimize_cases=[ B1R H1R;
    fprintf(fid, 'Width= %d \n', Optimize_cases(i,1) );
    fprintf(fid, 'Height= %d \n', Optimize_cases(i,2) );
    %Width=1; Height=1;

elseif strcmp (crossection, 'Circle')
    %Optimize_cases=[ R1Circle;
    fprintf(fid, 'Radius= %d \n', Optimize_cases(i,1) );
    %Radius=1;

elseif strcmp (crossection, 'Chan')
    %Optimize_cases=[ B1C B1C H1C TF1C TF1C TW1C;
    fprintf(fid, 'W1= %d \n', Optimize_cases(i,1) );
    fprintf(fid, 'W2= %d \n', Optimize_cases(i,2) );
    fprintf(fid, 'W3= %d \n', Optimize_cases(i,3) );
    fprintf(fid, 'T1= %d \n', Optimize_cases(i,4) );
    fprintf(fid, 'T2= %d \n', Optimize_cases(i,5) );
    fprintf(fid, 'T3= %d \n', Optimize_cases(i,6) );
    %W1=1; W2=2; W3=3; T1=1; T2=2; T3=1;

elseif strcmp (crossection, 'Z')
    %Optimize_cases=[ B1Z B1Z H1Z TF1Z TF1Z TW1Z;
    fprintf(fid, 'W1= %d \n', Optimize_cases(i,1) );
    fprintf(fid, 'W2= %d \n', Optimize_cases(i,2) );
    fprintf(fid, 'W3= %d \n', Optimize_cases(i,3) );
    fprintf(fid, 'T1= %d \n', Optimize_cases(i,4) );
    fprintf(fid, 'T2= %d \n', Optimize_cases(i,5) );
    fprintf(fid, 'T3= %d \n', Optimize_cases(i,6) );
    %W1=1; W2=2; W3=3; T1=1; T2=2; T3=1;

```

```

elseif strcmp (crossection , 'L')
%Optimize_cases=[ B1L    H1L    TF1L    TW1L;
fprintf(fid , 'W1= %d \n' , Optimize_cases(i,1) );
fprintf(fid , 'W3= %d \n' , Optimize_cases(i,2) );
fprintf(fid , 'T1= %d \n' , Optimize_cases(i,3) );
fprintf(fid , 'T3= %d \n' , Optimize_cases(i,4) );
%W1=1; W3=3; T1=1; T3=1;

elseif strcmp (crossection , 'T')
%Optimize_cases=[ B1L    H1L    TF1L    TW1L;
fprintf(fid , 'W1= %d \n' , Optimize_cases(i,1) );
fprintf(fid , 'W3= %d \n' , Optimize_cases(i,2) );
fprintf(fid , 'T1= %d \n' , Optimize_cases(i,3) );
fprintf(fid , 'T3= %d \n' , Optimize_cases(i,4) );
%W1=1; W3=3; T1=1; T3=1;

elseif strcmp (crossection , 'Half_circle')
%Radius=1; angle_inner=1; Radius_inner=1; angle=1;
fprintf(fid , 'R1= %d \n' , Optimize_cases(i,1) );
fprintf(fid , 'T1= %d \n' , Optimize_cases(i,2) );
fprintf(fid , 'ALFA1= %d \n' , Optimize_cases(i,3) );

elseif strcmp (crossection , 'Elips')
%Radius=1; angle_inner=1; Radius_inner=1; angle=1;

elseif strcmp (crossection , 'Circular_tube')

elseif strcmp (crossection , 'I')
%Optimize_cases=[ B1l    B1l    H1l    TF1l    TF1l    TW1l;
fprintf(fid , 'W1= %d \n' , Optimize_cases(i,1) );
fprintf(fid , 'W2= %d \n' , Optimize_cases(i,2) );
fprintf(fid , 'W3= %d \n' , Optimize_cases(i,3) );
fprintf(fid , 'T1= %d \n' , Optimize_cases(i,4) );
fprintf(fid , 'T2= %d \n' , Optimize_cases(i,5) );
fprintf(fid , 'T3= %d \n' , Optimize_cases(i,6) );
%W1=1; W2=2; W3=3; T1=1; T2=2; T3=1;

elseif strcmp (crossection , 'Rect_tube')
%Optimize_cases=[ B1R    H1R    TF1R    TF1R    TW1R    TW1R;
fprintf(fid , 'W1= %d \n' , Optimize_cases(i,1) );
fprintf(fid , 'W3= %d \n' , Optimize_cases(i,2) );
fprintf(fid , 'T1= %d \n' , Optimize_cases(i,3) );
fprintf(fid , 'T2= %d \n' , Optimize_cases(i,4) );
fprintf(fid , 'T3= %d \n' , Optimize_cases(i,5) );
fprintf(fid , 'T4= %d \n' , Optimize_cases(i,6) );
%W1=1; W3=3; T1=1; T2=2; T3=1; T4=1;

elseif strcmp (crossection , 'Hat')
%Optimize_cases=[ B1Z    B1Z    H1Z    TF1Z    TF1Z    TW1Z;
fprintf(fid , 'W1= %d \n' , Optimize_cases(i,1) );
fprintf(fid , 'W2= %d \n' , Optimize_cases(i,2) );
fprintf(fid , 'W3= %d \n' , Optimize_cases(i,3) );
fprintf(fid , 'W4= %d \n' , Optimize_cases(i,4) );
fprintf(fid , 'T1= %d \n' , Optimize_cases(i,5) );
fprintf(fid , 'T2= %d \n' , Optimize_cases(i,6) );
fprintf(fid , 'T3= %d \n' , Optimize_cases(i,7) );

```

```

        fprintf(fid , 'T4= %d \n' , Optimize_cases(i,8) );
        fprintf(fid , 'T5= %d \n' , Optimize_cases(i,9) );
        %W1=1; W2=2; W3=3; T1=1; T2=2; T3=1;

elseif strcmp (crossection , 'IHat')
    %Optimize_cases=[ B1Z B1Z H1Z TF1Z TF1Z TW1Z;
        fprintf(fid , 'W1= %d \n' , Optimize_cases(i,1) );
        fprintf(fid , 'W2= %d \n' , Optimize_cases(i,2) );
        fprintf(fid , 'W3= %d \n' , Optimize_cases(i,3) );
        fprintf(fid , 'W4= %d \n' , Optimize_cases(i,4) );
        fprintf(fid , 'T1= %d \n' , Optimize_cases(i,5) );
        fprintf(fid , 'T2= %d \n' , Optimize_cases(i,6) );
        fprintf(fid , 'T3= %d \n' , Optimize_cases(i,7) );
        fprintf(fid , 'T4= %d \n' , Optimize_cases(i,8) );
        fprintf(fid , 'T5= %d \n' , Optimize_cases(i,9) );
        %W1=1; W2=2; W3=3; T1=1; T2=2; T3=1;
end
fclose(fid);true

%% Startup ansys with "run_ansys" --> which starts ansys and runs "
Warping_shell_maurice_v3"
cd 'D:\tudelft 2019-2020\Thesis project -\software\Ansys\
Warping_shell_maurice_v3'
!run_ansys.bat
% within starting up ansys, make sure the following is checked:
% 1: see if the correct material properties are checked
% 2: make sure the vpn is working!!!!

%pause(10)

%% Post processing --> getting data from ansys
% index 1= rotx index 2= ux Index 3= total energy
% Index 4= max stress Index 5= ( moment x)

%% Save rotation data ansys
if strcmp ( Loading , 'Rotation')
% index 1= x position , index 2= Area Index 3= Rotx
% Index 4= X moment Index 5= Bimoment Index 6= Bicurvature
% Index 7= Energy Index 8= Maximum stress
%index_name= [ "Angle-eff" , "x-pos" , "Area" , "Rotx" , "X-mom" , "Bi-m
" , "Bi-c" ];

% when opening example=matfile('as.mat'); C=example.matrix;
if strcmp (crossection , 'Rectangle')
load Output_Ansys_Rectangle.txt;
Results_ansys(:, :, i)=[Output_Ansys_Rectangle];
save('Output_matlab_Rectangle_Rotation_Shell.mat', 'Results_ansys')

elseif strcmp (crossection , 'Chan')
load Output_Ansys_Chan.txt;
Results_ansys(:, :, i)= [Output_Ansys_Chan];
save('Output_matlab_Chan_Rotation_Shell.mat', 'Results_ansys')

elseif strcmp (crossection , 'Z')
load Output_Ansys_Z.txt;
Results_ansys(:, :, i)=[Output_Ansys_Z];

```

```

save('Output_matlab_Z_Rotation_Shell.mat', 'Results_ansys')

elseif strcmp (crossection, 'L')
load Output_Ansys_L.txt;
Results_ansys(:, :, i) = [Output_Ansys_L];
save('Output_matlab_L_Rotation_Shell.mat', 'Results_ansys')

elseif strcmp (crossection, 'T')
load Output_Ansys_T.txt;
Results_ansys(:, :, i) = [Output_Ansys_T];
save('Output_matlab_T_Rotation_Shell.mat', 'Results_ansys')

elseif strcmp (crossection, 'Half_circle')
load Output_Ansys_Half_circle.txt;
Results_ansys(:, :, i) = [Output_Ansys_Half_circle];
save('Output_matlab_Half_circle_Rotation_Shell.mat', 'Results_ansys')

elseif strcmp (crossection, 'I')
load Output_Ansys_I.txt;
Results_ansys(:, :, i) = [Output_Ansys_I];
save('Output_matlab_I_Rotation_Shell.mat', 'Results_ansys')

elseif strcmp (crossection, 'Rect_tube')
load Output_Ansys_Rect_tube.txt;
Results_ansys(:, :, i) = [Output_Ansys_Rect_tube];
save('Output_matlab_Rect_tube_Rotation_Shell.mat', 'Results_ansys')

elseif strcmp (crossection, 'Hat')
load Output_Ansys_Hat.txt;
Results_ansys(:, :, i) = [Output_Ansys_Hat];
save('Output_matlab_Hat_Rotation_Shell.mat', 'Results_ansys')

elseif strcmp (crossection, 'IHat')
load Output_Ansys_IHat.txt;
Results_ansys(:, :, i) = [Output_Ansys_IHat];
save('Output_matlab_IHat_Rotation_Shell.mat', 'Results_ansys')
end

%% Save torque data ansys
elseif strcmp (Loading, 'Torque')
% looking into moment transfer
% index 1= x position,      index 2= Area      Index 3= Rotx
% Index 4= X moment      Index 5= Bimoment  Index 6= Bicurvature
% Index 7= Energy      Index 8= Maximum stress
%index_name= [ "Angle-eff" , "torque-eff" , "x-pos" , "Area" , "Rotx" , "X
-mom" , "Bi-m" , "Bi-c" ];

if strcmp (crossection, 'Rectangle')
load Output_Ansys_Rectangle.txt;
Results_ansys(:, :, i) = [Output_Ansys_Rectangle];
save('Output_matlab_Rectangle_Torque_Shell.mat', 'Results_ansys')

%elseif crossection== 'Circle'

elseif strcmp (crossection, 'Chan')
load Output_Ansys_Chan.txt;

```

```
Results_ansys(:,:,i)= [Output_Ansys_Chan];
save('Output_matlab_Chan_Torque_Shell.mat','Results_ansys')

elseif strcmp (crossection, 'Z')
load Output_Ansys_Z.txt;
Results_ansys(:,:,i)= [Output_Ansys_Z];
save('Output_matlab_Z_Torque_Shell.mat','Results_ansys')

elseif strcmp (crossection, 'L')
load Output_Ansys_L.txt;
Results_ansys(:,:,i)= [Output_Ansys_L];
save('Output_matlab_L_Torque_Shell.mat','Results_ansys')

elseif strcmp (crossection, 'T')
load Output_Ansys_T.txt;
Results_ansys(:,:,i)= [Output_Ansys_T];
save('Output_matlab_T_Torque_Shell.mat','Results_ansys')

elseif strcmp (crossection, 'Half_circle')
load Output_Ansys_Half_circle.txt;
Results_ansys(:,:,i)= [Output_Ansys_Half_circle];
save('Output_matlab_Half_circle_Torque_Shell.mat','Results_ansys')

elseif strcmp (crossection, 'I')
load Output_Ansys_I.txt;
Results_ansys(:,:,i)= [Output_Ansys_I];
save('Output_matlab_I_Torque_Shell.mat','Results_ansys')

elseif strcmp (crossection, 'Rect_tube')
load Output_Ansys_Rect_tube.txt;
Results_ansys(:,:,i)= [Output_Ansys_Rect_tube];
save('Output_matlab_Rect_tube_Torque_Shell.mat','Results_ansys')

elseif strcmp (crossection, 'Hat')
load Output_Ansys_Hat.txt;
Results_ansys(:,:,i)= [Output_Ansys_Hat];
save('Output_matlab_Hat_Torque_Shell.mat','Results_ansys')

elseif strcmp (crossection, 'IHat')
load Output_Ansys_IHat.txt;
Results_ansys(:,:,i)= [Output_Ansys_IHat];
save('Output_matlab_IHat_Torque_Shell.mat','Results_ansys')
end

end

end
```

!!!!!!!!!!!!!! Warping beam analysis for different cross sections  
! Maurice Valentijn

!!!!!!!!!!!!!! General info

```
/CWD, 'D:\tudelft 2019-2020\Thesis project -\software\Ansys\
Warping_shell_maurice_v3'
finish
/clear, start
/title, Warping_shell_maurice_v3
/FILNAME, Warping_shell_maurice_v3,1
/CONFIG, NRES, 100000 ! assigns values to ansys
configuration manager, "nres" is the parameter to be changed
*Abbr, Gplot, gplot ! defines an abbreviation,
makes them appear in the tool box bar
*Abbr, Deformed, pldisp,1 ! displays the displaced structure,
makes them appear in the tool box bar
*Abbr, Input, /input, Warping_shell_maurice_v3
/eshape,1 ! Displays
elements with shapes determined from the real constants,
/nerr,,,,Off, !Negates all errors given
by ansys during /input

/units, SI
```

!!!!!!!!!!!!!! PARAMETERS definitions

```
pi = 3.14159265
Poisson = 0.41
Elastmod = 1.2e9 !youngs modulus --> Materialise says
1700-1800MPa
Gmod = 0.43e9
Density = 1010!7800
! Pure aluminium, Density=2.70e3, Poisson=0.33, Elastmod
=70.5e9, Gmod=26e9, yield strength=48e6
! 70 series aluminium, Density=2.85e3, Poisson=0.33, Elastmod
=71e9, Gmod=27.5e9, yield strength=427e6
! Average steel, Density=7.8e3, Poisson=0.29,
Elastmod=200e9, Gmod=77e9, yield strength
=310e6
! Average polupropylene, Density=900, Poisson=0.398, Elastmod
=1.7e9, Gmod=0.6e9, yield strength=35e6

! Average polyamide Density=1.01e3 Poisson=0.41, Elastmod
=1.2e9, Gmod=0.43e9, yield strength=38e6, UTS
48e6
```

! Matlab input section

```
/input, 'Ansys_input_crossection', 'txt'
! parameters from
```

!!!!!!!!!!!!!! cross section shap

```
!crossection = 'I' ! 'Rectangle' 'Circle' '
Circular_tube' 'I_profile' 'Rect_tube' 'Chan' 'Z' 'L' '
Half_circle' 'Elips' 'Hat' 'T'
```

```

!Loading= 'Torque' ! 'Torque' 'Rotation'
construction = 'continuous' ! 'continuous' or 'discrete'

!!!!!!!!!!!! twist load case
!steps=5
!theta_min=0
theta_max=pi/4 !pi/4
!theta_step=(theta_max-theta_min)/(steps-1)

!moment_min=0
moment_max=0.4/2 !20
!moment_step=(moment_max-moment_min)/(steps-1)

!!!!!!!!!!!! /prep7 enters the general data preprocessor
/prep7
! making a beam with the properties given before
ET, 1, shell181 !shell181 !beam188 ! defines a local element
type from the library (ET, ITYPE, Ename, KOP1, KOP2)
mp, ex, 1, Elastmod !Defines a linear material
property as a constant or a function of temperature.
mp, nuxy, 1, Poisson
!mp, gxy, 1, Gmod
mp, dens,1,Density

*if, crossection, EQ, 'Rectangle', THEN
!
!
!
*elseif, crossection, EQ, 'Chan'
! define keypoints
x0=0
y0=0 ! height
z0=0 ! width

length =360e-3
t1=T1 ! comes from matlab t= thickness all all flanges
y1=W3/2 ! comes from matlab y= the height of the beam
z1=W1/2 ! comes from matlab z= the width of the flanges
x2=length
k,1, x0, y1, z0
k,2, x0, y1, z1
k,3, x0, y1, -z1
k,4, x0, -y1, z0
k,5, x0, -y1, z1
k,6, x0, -y1, -z1
k,7, x2, y1, z0

! define lines , material , secnum,lmesh
l,2,3
l,3,6
l,5,6
l,1,7

!!!!!!!!!!!!!! USED TO CREATE CHANNEL BEAM
FLST,2,3,4,ORDE,2

```

```

FITEM,2,1
FITEM,2,-3
ADRAG,P51X, , , , , 4

! get rid of extra lines/nodes
NUMMRG,KP, , , ,LOW

! create crosssection
sect,1,shell, ,
secdata, t1,1,0.0,3
secoffset,MID
seccontrol, , , , , ,

! To couple the different areas
NUMMRG,ALL

! meshing
FLST,5,4,4,ORDE,4
FITEM,5,6
FITEM,5,-7
FITEM,5,9
FITEM,5,11
CM,_Y,LINE
LSEL, , , ,P51X
CM,_Y1,LINE
CMSEL, ,_Y
LESIZE,_Y1, , ,40, , , , ,1
FLST,5,4,4,ORDE,4
FITEM,5,1
FITEM,5,3
FITEM,5,5
FITEM,5,10
CM,_Y,LINE
LSEL, , , ,P51X
CM,_Y1,LINE
CMSEL, ,_Y
LESIZE,_Y1, , ,10, , , , ,1
FLST,5,2,4,ORDE,2
FITEM,5,2
FITEM,5,8
CM,_Y,LINE
LSEL, , , ,P51X
CM,_Y1,LINE
CMSEL, ,_Y
LESIZE,_Y1, , ,10, , , , ,1
MSHAPE,0,2D
MSHKEY,0
FLST,5,3,5,ORDE,2
FITEM,5,1
FITEM,5,-3
CM,_Y,AREA
ASEL, , , ,P51X
CM,_Y1,AREA
CHKMSH,'AREA'
CMSEL,S,_Y
AMESH,_Y1

```

```

CMDELE,_Y
CMDELE,_Y1
CMDELE,_Y2

! couple nodes to create a rigid zone
! input node to line
FLST,5,9,1,ORDE,2
FITEM,5,502
FITEM,5,-510
CM,_NODECM,NODE
*SET,_z1, 506
NSEL,S,,P51X
NSEL,A,,_Z1
CM,_CERGCM,NODE
CMSEL,S,_NODECM
!*
CMSEL,S,_CERGCM
CERIG,506,ALL,ALL,, , ,
CMSEL,S,_NODECM

! output node to line
FLST,5,9,1,ORDE,2
FITEM,5,453
FITEM,5,-461
CM,_NODECM,NODE
*SET,_z1, 457
NSEL,S,,P51X
NSEL,A,,_Z1
CM,_CERGCM,NODE
CMSEL,S,_NODECM
!*
CMSEL,S,_CERGCM
CERIG,457,ALL,ALL,, , ,
CMSEL,S,_NODECM

! keyopt statements

FINISH

/SOLU
                                antype, static                !static analysis
                                !nlgeom,on                    !nonlinear geometry
                                !autots, on                   !auto time-stepping
                                !outres,all,all               !save results of all iterations
                                !OUTPR,all,ALL,              !controls the solution print out

! Constraint middle point
D,686, ,0, , , ,ALL, , , ,

! Constraint web nodes
!D,32, ,0, , , ,UZ, , , ,
D,530, ,0, , , ,UZ, , , ,
D,569, ,0, , , ,UZ, , , ,
D,608, ,0, , , ,UZ, , , ,
D,647, ,0, , , ,UZ, , , ,

```

```

D,725, ,0, , , ,UZ, , , , ,
D,764, ,0, , , ,UZ, , , , ,
D,803, ,0, , , ,UZ, , , , ,
D,842, ,0, , , ,UZ, , , , ,
!D,482, ,0, , , ,UZ, , , , ,
! Constraint flange nodes
!D,159, ,0, , , ,UY, , , , ,
!D,237, ,0, , , ,UY, , , , ,
!D,315, ,0, , , ,UY, , , , ,
!D,393, ,0, , , ,UY, , , , ,

!D,1213, ,0, , , ,UY, , , , ,
!D,1135, ,0, , , ,UY, , , , ,
!D,1057, ,0, , , ,UY, , , , ,
!D,979, ,0, , , ,UY, , , , ,

! loading statement for theta
  *if, Loading, EQ, 'Rotation', THEN
    D,506, ,theta_max, , , ,ROTX, , , , ,

! Loading statement for moment
  *elseif, Loading, EQ, 'Torque'
    FLST,2,2,1,ORDE,2
    FITEM,2,506
    FITEM,2,457
    F,P51X,MX,moment_max

  *endif

solve

FINISH

!!!!!! enters the time history results postprocessor
/POST26
FINISH

/post1

*cfopen,Output_Ansys_Chan,txt !Create file

*GET,ROTX,node,457,rotx ! rotation around x axis
!*GET,MOMX,node,907,M11 ! measured torque around x axis
*GET,UX,node,1,ux ! displacement in in x direction

ETABLE,SENE,SENE ! Retrieve strain energy per element
SSUM ! Sum strain energy from ETABLE
*GET,TOT_ENERGY,SSUM,0,Item1,SENE ! Gets SENE from ETABLE and defines it
  as "my_Energy"

!PLNSOL, S,EQV, 0,1.0
!*GET,MAX_STRESS,PLNSOL,0,MAX !Maximum value of item in last contour
  display
! probably doesnt work because no visuals given

  *GET,MAX_STRESS,SECR,ALL,S,EQV,MAX

```

```

*CFWRITE, ,ROTX,UX,TOT_ENERGY,MAX_STRESS
*cfclos
!
!
!
*elseif, crossection, EQ, 'I'
! define keypoints
x0=0
y0=0 ! height
z0=0 ! width

length =360e-3
t1=T1 ! comes from matlab t= thickness all all flanges
y1=W3/2 ! comes from matlab y= the height of the beam
z1=W1/2 ! comes from matlab z= the width of the flanges
x2=length
k,1, x0, y1, z0
k,2, x0, y1, z1
k,3, x0, y1, -z1
k,4, x0, -y1, z0
k,5, x0, -y1, z1
k,6, x0, -y1, -z1
k,7, x2, y1, z0
k,8, x2, -y1, z0

! define lines, material, secnum,lmesh

I,1,2
I,1,3
I,1,4 ! THIS LINE FOR I BEAM
I,4,5
I,4,6
I,1,7
I,4,8 ! also needed for I

!!!!!!!!!! USED TO CREATE THE I BEAM!!
FLST,2,3,4,ORDE,3
FITEM,2,1
FITEM,2,3
FITEM,2,5
ADRAG,P51X, , , , , 6
ADRAG, 4, , , , , 7
ADRAG, 2, , , , , 6
!!!!!!!!!! END CREATING I BEAM

! get rid of extra lines/nodes
NUMMRG,KP, , , ,LOW

! create crossection
sect,1,shell, ,
secdata, t1,1,0.0,3
secoffset,MID
seccontrol, , , , , ,

! To couple the different areas

```

NUMMRG,ALL

```
! meshing
FLST,5,6,4,ORDE,6
FITEM,5,6
FITEM,5,-7
FITEM,5,9
FITEM,5,14
FITEM,5,17
FITEM,5,20
CM,_Y,LINE
LSEL,,,P51X
CM,_Y1,LINE
CMSEL, _Y
!*
LESIZE,_Y1,,,40,,,,,1
!*
FLST,5,8,4,ORDE,8
FITEM,5,1
FITEM,5,-2
FITEM,5,4
FITEM,5,-5
FITEM,5,8
FITEM,5,13
FITEM,5,15
FITEM,5,18
CM,_Y,LINE
LSEL,,,P51X
CM,_Y1,LINE
CMSEL, _Y
!*
LESIZE,_Y1,,,5,,,,,1
!*
FLST,5,2,4,ORDE,2
FITEM,5,3
FITEM,5,11
CM,_Y,LINE
LSEL,,,P51X
CM,_Y1,LINE
CMSEL, _Y
!*
LESIZE,_Y1,,,10,,,,,1
!*
MSHAPE,0,2D
MSHKEY,0
!*
FLST,5,5,5,ORDE,2
FITEM,5,1
FITEM,5,-5
CM,_Y,AREA
ASEL,,,P51X
CM,_Y1,AREA
CHKMSH,'AREA'
CMSEL,S,_Y
!*
AMESH,_Y1
```

```

!*
CMDELE,_Y
CMDELE,_Y1
CMDELE,_Y2
!*

NUMMRG,ALL

! couple nodes to create a rigid zone
FLST,5,9,1,ORDE,2
FITEM,5,297
FITEM,5,-305
CM,_NODECM,NODE
*SET,_z1,301
NSEL,S,,P51X
NSEL,A,,_Z1
CM,_CERGCM,NODE
CMSEL,S,_NODECM
!*
CMSEL,S,_CERGCM
CERIG,301,ALL,ALL,,
CMSEL,S,_NODECM

! output node to line
FLST,5,9,1,ORDE,2
FITEM,5,248
FITEM,5,-256
CM,_NODECM,NODE
*SET,_z1,252
NSEL,S,,P51X
NSEL,A,,_Z1
CM,_CERGCM,NODE
CMSEL,S,_NODECM
!*
CMSEL,S,_CERGCM
CERIG,252,ALL,ALL,,
CMSEL,S,_NODECM

! keyopt statements

FINISH

/SOLU
                                antype,static                                !static analysis
                                !nlgeom,on                                  !nonlinear geometry
                                !autots,on                                  !auto time-stepping
                                !outres,all,all                            !save results of all iterations
                                !OUTPR,all,ALL,                            !controls the solution print out

! Constraint middle point
D,481,,0,,,,,ALL,,,,

! Constraint web nodes
!D,27,,0,,,,,UZ,,,,,
D,325,,0,,,,,UZ,,,,,

```

```

D,364, ,0, , , ,UZ, , , , ,
D,403, ,0, , , ,UZ, , , , ,
D,442, ,0, , , ,UZ, , , , ,
D,520, ,0, , , ,UZ, , , , ,
D,559, ,0, , , ,UZ, , , , ,
D,598, ,0, , , ,UZ, , , , ,
D,637, ,0, , , ,UZ, , , , ,
!D,277, ,0, , , ,UZ, , , , ,
! Constraint flange nodes
!D,110, ,0, , , ,UY, , , , ,
!D,188, ,0, , , ,UY, , , , ,
!D,1174, ,0, , , ,UY, , , , ,
!D,1252, ,0, , , ,UY, , , , ,

!D,1047, ,0, , , ,UY, , , , ,
!D,969, ,0, , , ,UY, , , , ,
!D,764, ,0, , , ,UY, , , , ,
!D,842, ,0, , , ,UY, , , , ,
! Loading statements

! Loading statement theta
  *if , Loading, EQ, 'Rotation', THEN
    D,301, ,theta_max, , , ,ROTX, , , , ,

! Loading statement for moment
  *elseif , Loading, EQ, 'Torque'
    FLST,2,2,1,ORDE,2
    FITEM,2,301
    FITEM,2,252
    F,P51X,MX,moment_max

  *endif

solve

FINISH

!!!!!! enters the time history results postprocessor
/POST26
FINISH

/post1

*cfopen ,Output_Ansys_I ,txt !Create file

*GET,ROTX,node,252,rotx ! rotation around x axis
!*GET,MOMX,node,907,M11 ! measured torque around x axis
*GET,UX,node,2,ux ! displacement in in x direction

ETABLE,SENE,SENE ! Retrieve strain energy per element
SSUM ! Sum strain energy from ETABLE
*GET,TOT_ENERGY,SSUM,0,Item1,SENE ! Gets SENE from ETABLE and defines it
as "my_Energy"

*GET,MAX_STRESS,SECR,ALL , S,EQV,MAX

```

```

*CFWRITE, ,ROTX,UX,TOT_ENERGY,MAX_STRESS
*cfclos
!
!
!
*elseif, crossection, EQ, 'Z'
! define keypoints
x0=0
y0=0 ! height
z0=0 ! width

length =360e-3
t1=T1 ! comes from matlab t= thickness all all flanges
y1=W3/2 ! comes from matlab y= the height of the beam
z1=W1 ! comes from matlab z= the width of the flanges
x2=length
      k,1, x0, y1, z0
      k,2, x0, y1, z1

      k,4, x0, -y1, z0

      k,6, x0, -y1, -z1
      k,7, x2, y1, z0

! define lines, material, secnum,lmesh
l,2,1
l,1,4
l,4,6
l,1,7

!!!!!!!!!!!!!! USED TO CREATE Z BEAM
FLST,2,3,4,ORDE,2
FITEM,2,1
FITEM,2,-3
ADRAG,P51X, , , , , 4

! get rid of extra lines/nodes
NUMMRG,KP, , , ,LOW

! create crossection
sect,1,shell, ,
secdata, t1,1,0.0,3
secoffset,MID
seccontrol, , , , , ,

! To couple the different areas
NUMMRG,ALL

! meshing
FLST,5,4,4,ORDE,4
FITEM,5,4
FITEM,5,6
FITEM,5,9
FITEM,5,11
CM,_Y,LINE

```

```

LSEL, , , , P51X
CM, _Y1, LINE
CMSEL, , _Y
!*
LESIZE, _Y1, , , 40, , , , , 1
!*
FLST, 5, 6, 4, ORDE, 5
FITEM, 5, 1
FITEM, 5, -3
FITEM, 5, 5
FITEM, 5, 8
FITEM, 5, 10
CM, _Y, LINE
LSEL, , , , P51X
CM, _Y1, LINE
CMSEL, , _Y
!*
LESIZE, _Y1, , , 10, , , , , 1
!*
MSHAPE, 0, 2D
MSHKEY, 0
!*
FLST, 5, 3, 5, ORDE, 2
FITEM, 5, 1
FITEM, 5, -3
CM, _Y, AREA
ASEL, , , , P51X
CM, _Y1, AREA
CHKMSH, 'AREA'
CMSEL, S, _Y
!*
AMESH, _Y1
!*
CMDELE, _Y
CMDELE, _Y1
CMDELE, _Y2

! couple nodes to create a rigid zone
! input node to line
FLST, 5, 9, 1, ORDE, 2
FITEM, 5, 502
FITEM, 5, -510
CM, _NODECM, NODE
*SET, _z1, 506
NSEL, S, , , P51X
NSEL, A, , , _Z1
CM, _CERGCM, NODE
CMSEL, S, _NODECM
!*
CMSEL, S, _CERGCM
CERIG, 506, ALL, ALL, , , ,
CMSEL, S, _NODECM

! output node to line
FLST, 5, 9, 1, ORDE, 2
FITEM, 5, 453

```

```

FITEM,5,-461
CM,_NODECM,NODE
*SET,_z1, 457
NSEL,S,,P51X
NSEL,A,,_Z1
CM,_CERGCM,NODE
CMSEL,S,_NODECM
!*
CMSEL,S,_CERGCM
CERIG,457,ALL,ALL,,
CMSEL,S,_NODECM
! keyopt statements

FINISH

/SOLU
                                antype, static                !static analysis
                                !nlgeom,on                    !nonlinear geometry
                                !autots, on                   !auto time-stepping
                                !outres,all,all               !save results of all iterations
                                !OUTPR,all,ALL,              !controls the solution print out

! Constraint middle point
D,686, ,0, , , ,ALL, , , ,

! Constraint web nodes
!D,32, ,0, , , ,UZ, , , ,
D,530, ,0, , , ,UZ, , , ,
D,569, ,0, , , ,UZ, , , ,
D,608, ,0, , , ,UZ, , , ,
D,647, ,0, , , ,UZ, , , ,
D,725, ,0, , , ,UZ, , , ,
D,764, ,0, , , ,UZ, , , ,
D,803, ,0, , , ,UZ, , , ,
D,842, ,0, , , ,UZ, , , ,
!D,482, ,0, , , ,UZ, , , ,
! Constraint flange nodes
!D,159, ,0, , , ,UY, , , ,
!D,237, ,0, , , ,UY, , , ,
!D,315, ,0, , , ,UY, , , ,
!D,393, ,0, , , ,UY, , , ,

!D,1213, ,0, , , ,UY, , , ,
!D,1135, ,0, , , ,UY, , , ,
!D,1057, ,0, , , ,UY, , , ,
!D,979, ,0, , , ,UY, , , ,

! loading statement for theta
*if, Loading, EQ, 'Rotation', THEN
D,506, ,theta_max, , , ,ROTX, , , ,

! Loading statement for moment
*elseif, Loading, EQ, 'Torque'
FLST,2,2,1,ORDE,2
FITEM,2,506
FITEM,2,457

```

```
F, P51X, MX, moment_max

*endif

solve

FINISH

!!!!!! enters the time history results postprocessor
/POST26
FINISH

/post1

*cfdopen, Output_Ansys_Z, txt !Create file

*GET, ROTX, node, 457, rotx ! rotation around x axis
!*GET, MOMX, node, 907, M11 ! measured torque around x axis
*GET, UX, node, 1, ux ! displacement in in x direction

ETABLE, SENE, SENE ! Retrieve strain energy per element
SSUM ! Sum strain energy from ETABLE
*GET, TOT_ENERGY, SSUM, 0, Item1, SENE ! Gets SENE from ETABLE and defines it
as "my_Energy"

*GET, MAX_STRESS, SECR, ALL, S, EQV, MAX

*CFWRITE, , ROTX, UX, TOT_ENERGY, MAX_STRESS
*cfclos
!
!
!

!
!
!
*endif
```

